LBL-22247 c.2
Preprint

# Lawrence Berkeley Laboratory

UNIVERSITY OF CALIFORNIA

## Materials & Molecular Research Division

FEB 20 1987

Submitted to Journal of Chemical Physics

PHOTODISSOCIATION AS A QUANTUM TRANSITION: PHOTOFRAGMENT VIBRATIONAL DISTRIBUTIONS OF $C_2N_2(\tilde{C}\ ^1\Pi_u)$ PREDISSOCIATION

C.E. Dateo, V.Z. Kresin, M. Dupuis, and W.A. Lester, Jr.

October 1986

TWO-WEEK LOAN COPY

This is a Library Circulating Copy which may be borrowed for two weeks.

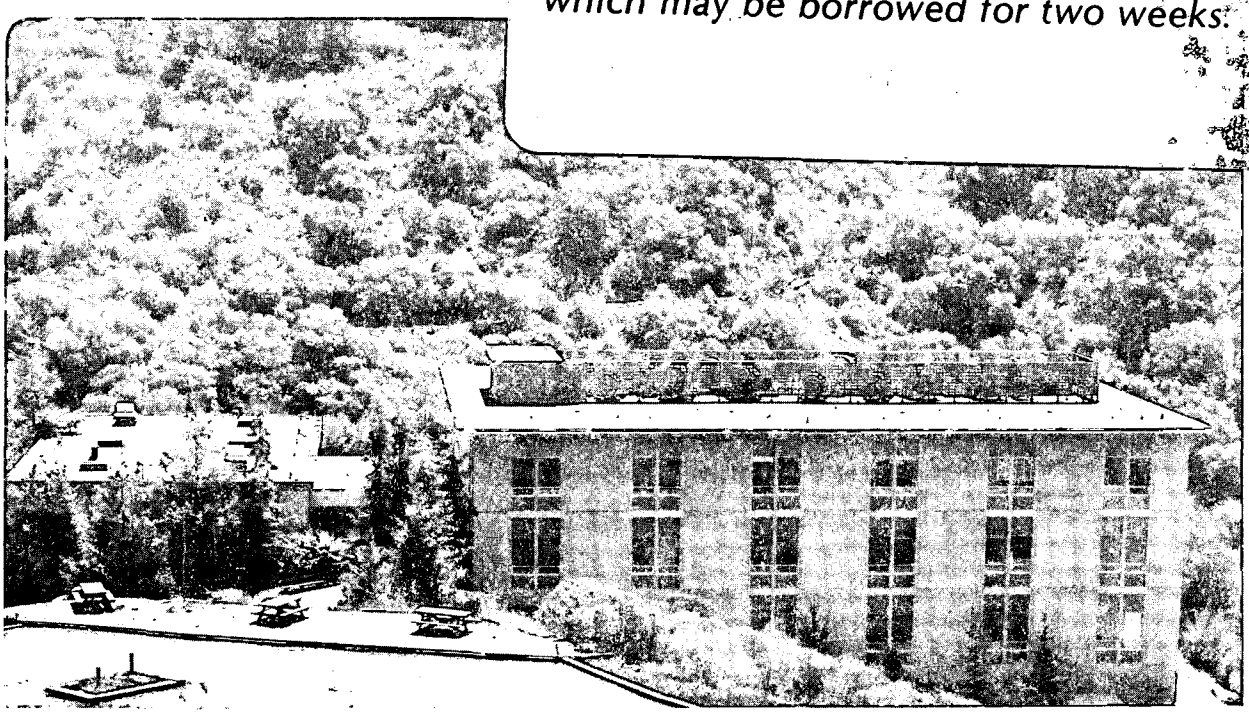

LBL-22247 c.2

Prepared for the U.S. Department of Energy under Contract DE-AC03-76SF00098

**DISCLAIMER**

This document was prepared as an account of work sponsored by the United States Government. While this document is believed to contain correct information, neither the United States Government nor any agency thereof, nor the Regents of the University of California, nor any of their employees, makes any warranty, express or implied, or assumes any legal responsibility for the accuracy, completeness, or usefulness of any information, apparatus, product, or process disclosed, or represents that its use would not infringe privately owned rights. Reference herein to any specific commercial product, process, or service by its trade name, trademark, manufacturer, or otherwise, does not necessarily constitute or imply its endorsement, recommendation, or favoring by the United States Government or any agency thereof, or the Regents of the University of California. The views and opinions of authors expressed herein do not necessarily state or reflect those of the United States Government or any agency thereof or the Regents of the University of California.

LBL-22247

# Photodissociation As A Quantum Transition: Photofragment Vibrational Distributions Of $C_2N_2(\tilde{C}\ ^1\Pi_u)$ Predissociation*

**C. E. Dateo†, V. Z. Kresin, M. Dupuis‡, and W. A. Lester, Jr.†**

*Materials and Molecular Research Division*
*Lawrence Berkeley Laboratory*
*University of California*
*Berkeley, California 94720*

## Abstract

Polyatomic indirect photodissociation is treated as a quantum transition between quasidiscrete and dissociative (photofragment) states. Our adiabatic method is followed to describe the nuclear dynamics of the dissociative state. *Ab initio* MCHF excited electronic potential energy surfaces are constructed and used to determine heavy-particle dynamics. The theory is applied to single-photon predissociation of $C_2N_2(\tilde{C}\ ^1\Pi_u)$ at 164, 158.7, and 153.6 nm to form $CN(X\ ^2\Sigma^+) + CN(A\ ^2\Pi)$. Theoretical predictions are found to be in good agreement with recent experimental product vibrational energy distributions.

*This work was supported by the Director, Office of Energy Research, Office of Basic Energy Sciences, Chemical Sciences Division of the U. S. Department of Energy under contract No. DE-AC03-76SF00098.

†Also, Department of Chemistry, University of California, Berkeley, California 94720.

‡Present Address, IBM Research Laboratory, Kingston, New York 12401.

## I. Introduction

Most theoretical treatments of polyatomic photodissociation have been limited to triatomic systems [1]. Some are based on the formal theory of scattering and lead to the necessity of solving sets of coupled differential or integral equations [2-7]. Such methods present well-known computational difficulties and become prohibitively difficult with the size of the polyatomic system. Approximations in formal scattering approaches can lead to simpler expressions requiring evaluation of a Franck-Condon (FC) matrix element [8-10]. Other FC approaches arise from perturbation theory [11-14]. Various FC methods have been found to yield reliable relative product energy distributions for direct single-photon photodissociation [15-20], but present difficulties in obtaining accurate absolute distributions. In this paper consideration is directed to indirect photodissociation which presents even more fundamental complications [1e].

Recent experimental studies [21-24] of cyanogen ($C_2N_2$) photodissociation have shown that the $\tilde{C}\ ^1\Pi_u$ state predissociates via a radiationless transition to ground state CN($X\ ^2\Sigma^+$) and electronically excited CN($A\ ^2\Pi$) fragments and have reported product vibrational distributions (PVDs) at several photon energies. An adiabatic correlation analysis identifies the predissociation as type II (vibrational), see below, which occurs on a single adiabatic electronic potential energy surface (PES). Although indirect photodissociation has been discussed in the theoretical literature [9,25-26], most computational studies have treated triatomic systems.

In this paper we focus on the evaluation of photofragment PVDs using an adiabatic theory of polyatomic photodissociation developed by two of us [12-14]. The theory treats indirect photodissociation as a quantum transition

between quasiadiabatic (diabatic) states [27-31] and leads to a localized description of the excited electronic adiabatic PES. Obtaining PVDs in this approach requires the evaluation of a FC-type factor. The method includes important contributions from final-state interactions [14], i.e., the translational-vibrational coupling in the dissociative channel. This contrasts with other FC approaches which neglect final-state interactions in the zeroeth-order approximation and include this coupling via a second step distorting the zeroeth-order solution.

This paper is organized as follows. In section II we summarize the theory, which has been presented in detail elsewhere [12-14]. Section III outlines the application of the approach to predissociation of $C_2N_2(\tilde{C}\ ^1\Pi_u)$ and compares computed and measured fragment PVDs. A summary and concluding remarks comprise section IV.

## II. Theory

### *Photodissociation as a Quantum Transition*

Indirect photodissociation occurs when absorption of radiation leaves the molecule in an excited electronic state of finite lifetime that subsequently undergoes a radiationless transition (predissociation) to a final dissociative state. Herzberg distinguishes three types of predissociation [32]: electronic (type I), vibrational (type II), and rotational (type III). Type I is accompanied by a change of PES, whereas types II and III occur on the same adiabatic electronic PES. For the latter cases, dissociation is caused by redistribution of vibrational or rotational energy of the molecule to translational and internal degrees of freedom of the fragments. Because of the finite lifetime of the excited state, it is a good approximation to neglect any dependence on the

electronic ground state and photon energy other than the specification of the transition.

The general theory of quantum transitions is well-known and appears in several quantum texts [33]. We summarize here the first-order perturbation theory analysis for the present application, and note that the method is valid to any order (see Appendix A). The probability of a radiationless transition from a quasidiscrete state (Q) to a dissociative state (D) is given by the golden rule expression

$$dW_{D\leftarrow Q} = \frac{2\pi}{\hbar} \left| H'_{D\leftarrow Q} \right|^2 \delta(E'-E)\, \rho_E\, dE, \tag{1}$$

where

$$H'_{D\leftarrow Q} = \int \Psi_D^*(\vec{r}, \vec{R})\ \hat{H}'\ \Psi_Q(\vec{r}, \vec{R})\, d\vec{R}\, d\vec{r}. \tag{2}$$

Here $\hat{H}'$ is the perturbation operator which governs the transition, $\rho_E$ is the density of states, $\Psi_D$ and $\Psi_Q$ are the total wave functions for the D and Q states, and $\vec{r}$ and $\vec{R}$ refer to the electronic and nuclear coordinates. To calculate the probability of a D←Q transition it is necessary to obtain expressions for $\hat{H}'$, $\Psi_D$, and $\Psi_Q$.

The applicability of the quantum theory of transitions arises from the capability of identifying that part of the total Hamiltonian, $\hat{H}'$, which causes the transition. For direct photodissociation it is the matter-radiation interaction which is the pertinent term of the Hamiltonian [33]. For type I indirect photodissociation, $\hat{H}'$ is the deviation from the Born-Oppenheimer (BO) approximation resulting from the neglect of nuclear motion (or spin-orbit coupling if the states are of different spin) [33]. For type II (vibrational) and type III (rotational) predissociation, the transition from the initial Q state to the final D photofragment state takes place on a single adiabatic PES. In the

former case we employ our method developed to treat chemical reaction as a quantum transition [34-35]. Type III predissociation could be treated similarly. Transformation to a diabatic representation yields a localized description of the quantum transition between two diabatic PESs. In this representation there are direct coupling terms which cause the transition between the diabatic states.

*Diabatic Representation*

The total Schrödinger equation can be written

$$\hat{H}\,\Psi(\vec{r},\vec{R}) = (\hat{H}_e + \hat{T}_{\vec{R}})\,\Psi(\vec{r},\vec{R}) = E\,\Psi(\vec{r},\vec{R}), \tag{3}$$

where $\hat{T}_{\vec{R}}$ is the nuclear kinetic energy operator and $\hat{H}_e$ is the electronic Hamiltonian

$$\hat{H}_e = \hat{T}_{\vec{r}} + V(\vec{r},\vec{R}). \tag{4}$$

Here $\hat{T}_{\vec{r}}$ is the electronic kinetic energy operator and $V(\vec{r},\vec{R})$ is the total potential energy. In accord with the BO approximation, the electronic wave function is defined by

$$\hat{H}_e\,\psi_n(\vec{r};\vec{R}) = \epsilon_n(\vec{R})\,\psi_n(\vec{r};\vec{R}). \tag{5}$$

The term $\epsilon_n(\vec{R})$ represents the nth adiabatic electronic PES and labels both the excited $C_2N_2$ molecule (Q state) and the photofragments (D state). We introduce a new potential $\tilde{V}(\vec{r},\vec{R})$, constructed so that the D←Q process is a surface crossing in the diabatic representation, i.e., the effect of substituting $\tilde{V}(\vec{r},\vec{R})$ for $V(\vec{r},\vec{R})$ in the electronic Schrödinger equation (5) is to change the adiabatic PESs $\epsilon_n(\vec{R})$ and $\epsilon_{n+1}(\vec{R})$ to diabatic PESs $\tilde{\epsilon}_Q(\vec{R})$ and $\tilde{\epsilon}_D(\vec{R})$ that are solutions to

$$\begin{bmatrix} \hat{T}_r + \tilde{V}(\vec{r}, \vec{R}) \end{bmatrix} \tilde{\psi}_Q(\vec{r}; \vec{R}) = \tilde{\epsilon}_Q(\vec{R})\, \tilde{\psi}_Q(\vec{r}; \vec{R})$$
$$\begin{bmatrix} \hat{T}_r + \tilde{V}(\vec{r}, \vec{R}) \end{bmatrix} \tilde{\psi}_D(\vec{r}; \vec{R}) = \tilde{\epsilon}_D(\vec{R})\, \tilde{\psi}_D(\vec{r}; \vec{R}). \tag{6}$$

More specifically, we choose the potential $\tilde{V}(\vec{r}, \vec{R})$ such that the term $\tilde{\epsilon}_Q(\vec{R})$ corresponds to the Q (predissociative) channel and is equivalent to $\epsilon_n(\vec{R})$ for small interfragment distances, $\rho$, and becomes $\epsilon_{n+1}(\vec{R})$ in the asymptotic region $\rho \rightarrow \infty$; similarly, $\tilde{\epsilon}_D(\vec{R})$ is equivalent to $\epsilon_n(\vec{R})$ for large $\rho$ as shown in Fig. 1.

Formally, one can introduce the total wave functions $\tilde{\Psi}_Q(\vec{r}, \vec{R}) = \tilde{\psi}_Q(\vec{r}; \vec{R})\, \tilde{\phi}_Q(\vec{R})$ and $\tilde{\Psi}_D(\vec{r}, \vec{R}) = \tilde{\psi}_D(\vec{r}; \vec{R})\, \tilde{\phi}_D(\vec{R})$, that are eigenfunctions of the total Hamiltonian

$$\tilde{H} = \hat{T}_R + \hat{T}_r + \tilde{V}(\vec{r}, \vec{R}) = \hat{T}_R + \tilde{H}_e \tag{7}$$

in a diabatic representation and lead to a PES crossing between the Q and D diabatic states. In the BO approximation, the diabatic nuclear wave functions are solutions of

$$\begin{bmatrix} \hat{T}_R + \tilde{\epsilon}_Q(\vec{R}) \end{bmatrix} \tilde{\phi}_Q(\vec{R}) = E\, \tilde{\phi}_Q(\vec{R})$$
$$\begin{bmatrix} \hat{T}_R + \tilde{\epsilon}_D(\vec{R}) \end{bmatrix} \tilde{\phi}_D(\vec{R}) = E\, \tilde{\phi}_D(\vec{R}). \tag{8}$$

This choice of diabatic representation yields a localized description of PESs. The function $\tilde{\phi}_Q(\vec{R})$ (and, hence, $\tilde{\Psi}_Q(\vec{r}, \vec{R})$) is exponentially small in the D channel, and $\tilde{\phi}_D(\vec{R})$ (and $\tilde{\Psi}_D(\vec{r}, \vec{R})$) is exponentially small in the Q channel.

Note that the total Schrödinger equation (3) can be rewritten in the form

$$\hat{H}\, \Psi(\vec{r}, \vec{R}) = (\tilde{H} + \Delta H)\, \Psi(\vec{r}, \vec{R}) = E\, \Psi(\vec{r}, \vec{R}), \tag{9}$$

where $\tilde{H}$ is defined by (7), and

$$\Delta H = V(\vec{r}, \vec{R}) - \tilde{V}(\vec{r}, \vec{R}) = \hat{H}_e - \tilde{H}_e. \tag{10}$$

The operator, $\Delta H$ governs the D←Q transition given by Eq. (1). Note that $\Delta H$ does not depend on time and thus can only cause transitions between states of the same energy [33].

Using Eq. (6) and the orthogonality of $\tilde{\psi}_Q$ to $\tilde{\psi}_D$ the transition matrix element of Eq. (2) can be reduced to the form

$$H'_{D\leftarrow Q} = \int \tilde{\phi}_D^*(\vec{R})\, \tilde{\phi}_Q(\vec{R})\, L(\vec{R})\, d\vec{R}, \tag{11}$$

where

$$L(\vec{R}) = \int \tilde{\psi}_D^*(\vec{r}; \vec{R})\, \hat{H}_e\, \tilde{\psi}_Q(\vec{r}; \vec{R})\, d\vec{r}. \tag{12}$$

The function $L(\vec{R})$ contains relatively slowly varying functions of $\vec{R}$. The major contribution to the matrix element will come from the region of overlap of the nuclear wave functions. This region will encompass the crossing point, $\vec{R}_o$, of the diabatic PESs (which, in general, will include the transition state of the adiabatic PES). Thus we can approximate Eq. (11) by

$$H'_{D\leftarrow Q} = L(\vec{R}_o) \int \tilde{\phi}_D^*(\vec{R})\, \tilde{\phi}_Q(\vec{R})\, d\vec{R}. \tag{13}$$

Hence, determination of absolute photofragment energy distributions requires the evaluation of a multidimensional FC-type integral and an electronic factor, $L(\vec{R}_o)$. Evaluation of $L(\vec{R}_o)$ is not trivial; however, relative energy distributions can be obtained from just the FC-type integrals reducing the determination of product energy distributions to a problem involving only nuclear degrees of freedom.

Equation (13) is similar to expressions derived from scattering theory for chemical reactions [36-39]. However, the present approach is based on the theory of quantum transitions and is similar in spirit to Bardeen's treatment

of tunneling [40]. Since the golden rule given by Eq. (1) results from first-order time-dependent perturbation theory, all virtual transitions are neglected [41]. If higher-order corrections are important, the probability is given by an expression similar to Eq. (1), but with the matrix element $H'_{D\leftarrow Q}$ replaced by the T-matrix element connecting the Q and D states. These higher-order corrections correspond to virtual transitions to electronic states lying above the diabatic states. These terms contain products of FC factors resulting in additional orders of smallness, in a perturbative sense, and thus serve as a check of the applicability of Eq. (1). It is important to note here that the validity of the Eq. (1) depends on the product of the coupling matrix element and the characteristic time of the perturbation being small. Hence, Eq. (1) is valid even if $H'_{D\leftarrow Q}$ is large for sufficiently short characteristic times. Our treatment differs from those based on scattering theory which lead to a single FC factor [36,38].

*Adiabatic Approach to Nuclear Dynamics*

In order to evaluate the FC integral it is necessary to obtain expressions for the nuclear wave functions $\tilde{\phi}_Q$ and $\tilde{\phi}_D$, that are solutions to Eq. (8). In general, rotational motion is slower than translational and vibrational motion, thus the present analysis neglects rotational motion entirely. (Rotational motion can be included as an additional step in an adiabatic development.) The Q state can often be described in the harmonic approximation as a product of normal modes. If the absorption spectrum consists of a set of equidistant bands, the harmonic approximation should be accurate, otherwise it is necessary to include anharmonicity corrections.

One of the most difficult aspects in treating polyatomic photodissociation is the proper description of the D state wave function, $\tilde{\phi}_D(\rho, q_i^A, q_l^B)$, where

$q_i^A$ and $q_l^B$ are internal coordinates of fragments A and B. The complication arises because $\tilde{\phi}_D$ contains factors describing both discrete spectra corresponding to the internal motion of the individual photofragments, and continuous spectra associated with their relative motion. In general, there is strong coupling between these two types of motion and, unlike the Q state, the potential energy $U(\rho, q_i^A, q_l^B)$ for the D state cannot be expanded in a series of deviations of all variables from equilibrium. The reason is that $\rho$, the distance between the centers of mass of the two fragments, represents unbounded translational motion. The major contribution to the transition matrix element will come from the region of overlap of the nuclear wave functions, where it is necessary to take explicit account of the interfragment interaction.

Following the adiabatic method of reference [1e,14], the D state of a linear tetra-atomic molecule may be described by the wave function

$$\tilde{\phi}_D(\rho, q_i^A, q_l^B) = \phi_{rel}(\rho, q^A, q^B)\, \phi_{int}(\rho, q^A, q^B). \tag{14}$$

where $\phi_{rel}$ is the wave function for translational motion, and $\phi_{int}$ in the wave function for internal motion. This result was obtained following an adiabatic approach. A general expression is constructed from rigorous solutions in two adiabatic limits: (i) $\alpha \equiv \frac{\epsilon_{rel}}{\epsilon_{int}} >> 1$, relative motion fast compared to internal motion, and (ii) $\alpha << 1$, the opposite condition.

For case (i) ($\alpha >> 1$), one can use the clamped translational function approximation, for which it has been shown [14] that the fragment frequencies and bond lengths are constants and well approximated by isolated fragment or asymptotic (asy) values, i.e.,

$$\begin{aligned} \omega^i &\approx \omega_{asy} \\ q_o^i &\approx q_{asy}. \end{aligned} \tag{15}$$

Conceptually, case (ii) can be described as the slow formation of photofragments along the repulsive surface with adiabatic adjustment of frequencies and bond lengths. The wave function describing the internal motion depends parametrically on the interfragment distance $\rho$. This limit implies a minimum energy (reaction) path for the dissociative coordinate which can be defined mathematically as simultaneously satisfying the conditions,

$$\begin{aligned} &\frac{\partial U(\rho, q^A, q^B)}{\partial q^A}\bigg|_{q^A = q_o^{A''}(\rho)} = \frac{\partial U(\rho, q^A, q^B)}{\partial q^B}\bigg|_{q^B = q_o^{B''}(\rho)} = 0 \\ &\text{and} \qquad \frac{\partial U(\rho, q^A, q^B)}{\partial \rho} \neq 0. \end{aligned} \tag{16}$$

The relative motion part of $\tilde{\phi}_D$ (Eq. (14)) is the solution to

$$\left[ -\frac{\hbar^2}{2\mu}\frac{\partial^2}{\partial \rho^2} + U_{eff}(\rho, q^A, q^B) \right] \phi_{rel}(\rho, q^A, q^B) = E\, \phi_{rel}(\rho, q^A, q^B), \tag{17}$$

where $\mu$ is the reduced mass of the system,

$$\begin{aligned} U_{eff}(\rho, q^A, q^B) &= U(\rho, q_o^A(\rho), q_o^B(\rho)) + \epsilon_{int}(\rho) \\ \epsilon_{int}(\rho) &= (n_A + 1/2)\,\hbar\,\Omega^A(\rho) + (n_B + 1/2)\,\hbar\,\Omega^B(\rho), \end{aligned} \tag{18}$$

and $q_o^A(\rho)$ and $q_o^B(\rho)$ are determined by the conditions

$$\left( \frac{\partial U(\rho, q^A, q^B)}{\partial q^{A(B)}} \right)\bigg|_{q^{A(B)} = q_o^{A(B)}(\rho)} = 0. \tag{19}$$

The internal motion wave function, $\phi_{int}$ of Eq. (14) is given by

$$\phi_{int}(\rho, q^A, q^B) = \phi^A(Q_A(q^A, q^B, \rho))\, \phi^B(Q_B(q^A, q^B, \rho)), \tag{20}$$

where (in the harmonic approximation)

$$\phi^{A(B)} = \left( \frac{\Omega^{A(B)}(\rho)}{\pi \hbar} \right)^{1/4} \frac{1}{\sqrt{2^{n_{A(B)}}\, n_{A(B)}!}} \exp\left( - \frac{\Omega^{A(B)}(\rho)\, Q^2_{A(B)}(q^A, q^B, \rho)}{2\hbar} \right) \cdot H_{n_{A(B)}}\left( Q_{A(B)}(qa, qb, \rho) \sqrt{\frac{\Omega^{A(B)}(\rho)}{\hbar}} \right). \tag{21}$$

Here $Q_{A(B)}(q^A, q^B, \rho)$ are normal coordinates for internal motion of the D state, which asymptotically become individual bond stretches of each product fragment, and $H_{n_{A(B)}}$ is an $n_{A(B)}$-order Hermite polynomial. The explicit form of $Q_{A(B)}(q^A, q^B, \rho)$ is discussed in Sec. III. The frequencies $\Omega(\rho)$ and the bond lengths $q_o(\rho)$ depend on the interfragment distance and are in general different from their asymptotic values $\omega_{asy}$ and $q_{asy}$. Specifically, we have [14],

$$\begin{aligned} \Omega(\rho) &= \omega^i \left( \frac{\omega^{ii}(\rho)}{\omega^i} \right)^{\beta}; \quad \beta \equiv (\alpha + 1)^{-1} \\ q_o(\rho) &= q_o^i \left( \frac{q_o^{ii}(\rho)}{q^i} \right)^{\beta} \end{aligned} \tag{22}$$

where the superscripts refer to the limiting cases (i) and (ii) above.

The form of general solution for the D state nuclear wave function given by Eqs. (14,17-22) results from direct comparison of the solutions in the two adiabatic limits. In both limits the wave function $\tilde{\phi}_D$ is expressed as a product of two functions describing relative and internal motion of the fragments; moreover, the corresponding functions possess similar structure. The limiting cases differ only in the behavior of the vibrational frequencies and equilibrium bond lengths. For $\alpha \ll 1$, the frequencies and equilibrium bond lengths are functions of $\rho$; whereas, the opposite limit is characterized by constant values of these parameters. The similar structure for the solutions of the two limiting cases suggests it is reasonable to conclude that a continuous transition

occurs in proceeding from the case $\alpha << 1$ to $\alpha >> 1$ that is accompanied by a change of the dependence of $\omega^{ii}(\rho)$ and $q_o^{ii}(\rho)$ to $\omega^i \approx \omega_{asy}$ and $q_o^i \approx q_{asy}$; see Eq. (15). This change is described by the interpolation scheme of Eq. (22). The explicit solutions for the two adiabatic limits for a linear tetra-atomic system are given in Appendix B.

We emphasize that the interaction between the fragments is taken into account in two ways. First, the vibrational frequencies and reaction path bond lengths depend on the interfragment distance $\rho$. Second, the effective potential energy $U_{eff}$, describing the relative motion, contains the vibrational energy.

## III. Application and Results for $C_2N_2(\tilde{C}\ ^1\Pi_u)$

### *Experiment*

Recent experimental studies [21-24] have indicated that $C_2N_2(\tilde{C}\ ^1\Pi_u)$ undergoes predissociation at wavelengths between 164 nm and 154 nm resulting in $CN(X\ ^2\Sigma^+)$ and $CN(A\ ^2\Pi)$. Figure 2 shows a correlation diagram illustrating how the low-lying states of $C_2N_2$ adiabatically correlate to separated CN radicals for linear geometry. The three lowest-energy channels for dissociation and their thresholds are

$$\begin{aligned} C_2N_2 &\rightarrow CN(X\ ^2\Sigma^+) + CN(X\ ^2\Sigma^+) \quad 222.2\text{nm} \quad \text{I} \\ &\rightarrow CN(X\ ^2\Sigma^+) + CN(A\ ^2\Pi) \quad 184.7\text{nm} \quad \text{II} \\ &\rightarrow CN(A\ ^2\Pi) + CN(A\ ^2\Pi) \quad 157.9\text{nm} \quad \text{III.} \end{aligned} \tag{23}$$

For wavelengths between 164 and 184.7 nm earlier studies [21,23] have shown the ratio of $CN(A\ ^2\Pi)$ to $CN(X\ ^2\Sigma^+)$ to be nearly unity indicating that only channel II occurs. At shorter wavelengths this ratio was found to be greater than unity implying that channel III must contribute. From Fig. 2 it is seen

that channel II adiabatically correlates to $C_2N_2(\tilde{C}\ ^1\Pi_u)$ and as such is an example of type II (vibrational) predissociation. Dissociation via channel III involves different electronic PESs and thus is type I (electronic) predissociation.

Miller et al. [21] photolyzed $C_2N_2$ under collisionless conditions at 164, 158.7, and 153.6 nm and measured nascent $CN(X\ ^2\Sigma^+)$ vibrational populations using laser induced fluorescence (LIF). They reported the ratio of populations ($\beta$) of $\nu = 1$ to $\nu = 0$, and at all wavelengths found $\beta < 1$, but increasing with photon energy. Taherian et al. [22] measured the $CN(A\ ^2\Pi)$ vibrational distribution resulting from $F_2$ laser excitation of $C_2N_2$ at 157.6 nm. They reported a $CN(A\ ^2\Pi)$ vibrational population detected by $CN(X \leftarrow A)$ emission spectra and observed vibrational levels up to the thermodynamic limit of $\nu = 5$ in a bimodal distribution with peaks at $\nu = 0$ and $\nu = 2$.

*Diabatic States for* $C_2N_2(\tilde{C}\ ^1\Pi_u) \rightarrow CN(X\ ^2\Sigma^+) + CN(A\ ^2\Pi)$

As described in Sec. II, the Q and D state wave functions, $\tilde{\psi}_Q$, and $\tilde{\psi}_D$, are not eigenstates of the electronic Hamiltonian, $\hat{H}_e$, of the system but of a diabatic Hamiltonian $\tilde{H}_e$ consistent with the transformation $V(\vec{r}, \vec{R}) \rightarrow \tilde{V}(\vec{r}, \vec{R})$. In general, diabatic states result from a nondiagonal representation of $\hat{H}_e$, of which there may be several of physical interest. The adiabatic states are unique, however, resulting from the diagonalization of $\hat{H}_e$. Hence, diabatic and adiabatic representations are rigorously equivalent, and the problem lies in specifying the representation that provides the most useful physical description of the system [27-31].

Electronic structure studies of $C_2N_2(\tilde{C}\ ^1\Pi_u)$ indicate it is best described as an $n \rightarrow \pi^*$ excitation from the ground state $n^3\pi^8\pi^{*1}$ electronic configuration.

Here n represents a nitrogen atom lone-pair electron and $\pi^*$ is the lowest-lying unoccupied orbital [42]. The CN(A $^2\Pi$) radical results from the excitation of a $\pi$ electron into a half-filled $\sigma$ orbital localized on carbon. The CN(X $^2\Sigma^+$) + CN(A $^2\Pi$) supermolecule has an $n^4\pi^7\sigma^{*1}$ electronic configuration. The adiabatic electronic PES reflects this change in character for increasing $\rho$. In the diabatic representation, however, $C_2N_2(\tilde{C}\ ^1\Pi_u)$ dissociates to CN(X $^2\Sigma^+$) and a higher energy CN($^2\Pi$) state. Collinear approach of CN(X $^2\Sigma^+$) to CN(A $^2\Pi$) results in a repulsive diabatic surface because of the interaction of the two lone-pair electrons of carbon in the $A^2\Pi$ radical with the single lone-pair electron of carbon in the ground state fragment (see Figure 3). It is the interaction between these two diabatic PESs (i.e., the off-diagonal terms in the diabatic representation of $\hat{H}_e$) that leads to the predissociative nature of the adiabatic surface.

The diabatic surfaces for the quasidiscrete and dissociative states can be constructed using the *ab initio* multiconfiguration Hartree-Fock (MCHF) method. The $n \rightarrow \pi^*$ character of the $C_2N_2(\tilde{C}\ ^1\Pi_u)$ state and the $\pi \rightarrow \sigma^*$ character of the CN(X $^2\Sigma^+$) + CN(A $^2\Pi$) supermolecule can be obtained by restricting the orbital occupations in the respective MCHF wave functions. To construct an MCHF wave function that correctly describes the adiabatic surface, it is necessary to include all configurations obtained by distributing 14 electrons among both the lone-pair orbitals ($n_u$, $n_g$), the $\pi$ orbitals ($\pi_u$, $\pi_g$, $\pi_u^*$, $\pi_g^*$), and the CC bonding and antibonding orbitals ($\sigma_g$, $\sigma_u^*$) in all possible ways consistent with $^1\Pi_u$ symmetry. We denote this wave function as $MC[\sigma_g, n_u, n_g, \pi_u, \pi_g, \pi_u^*, \pi_g^*, \sigma_u^*]^{14}$ (or just simply MC14). The diabatic Q state is obtained by omitting those configurations which include excitations

out of the CC($\sigma_g$) or into the CC($\sigma_u^*$) orbitals. This restricts the $\sigma_g$ orbital to remain fully occupied and the $\sigma_u^*$ orbital to be empty. By this specification, the Q state wave function, MC[$n_u$, $n_g$, $\pi_u$, $\pi_g$, $\pi_u^*$, $\pi_g^*$]$^{12}$ (MC12), will not dissociate to adiabatic products but will retain its n $\rightarrow \pi^*$ character. Similarly, if the configurations which include excitations from the lone pair orbitals are neglected, forcing them to remain fully occupied, the D state wave function, MC[$\sigma_g$, $\pi_u$, $\pi_g$, $\pi_u^*$, $\pi_g^*$, $\sigma_u^*$]$^{10}$ (MC10) with $\pi \rightarrow \sigma^*$ character is obtained.

Following these ideas, the optimized molecular geometry, force constants, and harmonic frequencies have been obtained [42] for $C_2N_2(\tilde{C}\ ^1\Pi_u)$ in excellent agreement with experimental data. The absorption spectrum consists of an equidistant set of bands [21], and thus the quasidiscrete state nuclear wave function can be well approximated by a product of harmonic oscillator functions of the normal modes. Frequencies and normal coordinates were determined from force constants obtained from a minimum basis set (STO-3G) MC12 wave function. The results of these calculations are summarized in Table I.

Because it is not possible experimentally to obtain geometries and force constants of fragments along the reaction path, we also employ *ab initio* MCHF methods to determine this data needed to describe the D state in the FC overlap region. A simple relationship can be derived for specifying the minimum energy path of a tetra-atomic system using the method of Lagrange multipliers (see Appendix C).

Figure 4 displays the results of the D state MCHF calculations. We note a strong $\rho$-dependence for both photofragment equilibrium bond lengths and frequencies along the repulsive PES. For small $\rho$ the system resembles the

symmetric $C_2N_2$ supermolecule rather than distinct CN(X $^2\Sigma^+$) and CN(A $^2\Pi$) radicals. The normal mode analysis yields normal coordinates expressible as symmetric and asymmetric linear combinations of the localized fragment bond stretches similar to those of quasidiscrete $C_2N_2(\tilde{C}\ ^1\Pi_u)$. The CN photofragments remain indistinguishable until an abrupt symmetry breaking at $\rho = 3.2$ Å. There the fragments are distinct, the bond lengths differ, and by $\rho = 3.6$ Å the fragments have almost reached the equilibrium bond lengths and frequencies of isolated CN(X $^2\Sigma^+$) and CN(A $^2\Pi$). For larger $\rho$ a normal mode analysis gives normal coordinates primarily composed of the individual localized bond stretches. For small $\rho$ the normal mode corresponding to the symmetric CN stretch is found to correlate asymptotically to the ground state CN(X $^2\Sigma^+$) stretch, and that for the asymmetric CN stretch, which has the lower frequency, correlates to the excited state CN(A $^2\Pi$) stretch.

The quasidiscrete state nuclear wave function will be nonzero for a region near its equilibrium geometry ($\rho_o$, $q_o^A$, $q_o^B$). Therefore the main contributions to the FC overlap will also come from this region. For $C_2N_2(\tilde{C}\ ^1\Pi_u)$ $\rho_o = 2.656$ Å. As shown in Figure 4, the frequencies and bond lengths in this region are clearly not the same as those for the isolated fragments.

*Evaluation of the Franck-Condon Overlap Integral*

Obtaining relative product energy distributions requires evaluation of the multidimensional overlap integral of the quasidiscrete and dissociative state nuclear wave functions,

$$H'_{D\leftarrow Q} \sim \int \tilde{\phi}_D^*(\vec{R})\, \tilde{\phi}_Q(\vec{R})\, d\vec{R}. \tag{24}$$

In this paper we are primarily concerned with *vibrational distributions* of the CN(X $^2\Sigma^+$) and CN(A $^2\Pi$) fragments resulting from predissociation of $C_2N_2(\tilde{C}$

$^1\Pi_u$). Both the ground ($\tilde{X}\ ^1\Sigma_g^+$) and excited ($\tilde{C}\ ^1\Pi_u$) molecular states are linear and, as a further adiabatic approximation, we may neglect bending vibrations and rotations and limit the analysis to the collinear arrangement. The general theory is applicable to nonlinear polyatomics and is presented in detail in reference [12]. Evaluation of the fragment rotational distributions would, of course, require inclusion of the corresponding degrees of freedom.

In the harmonic approximation, the nuclear wave function describing the internal motion of the quasidiscrete $C_2N_2(\tilde{C}\ ^1\Pi_u)$ state is given by a product of three oscillator functions,

$$\tilde{\phi}_Q(\vec{R}) = \prod_{i=1}^{3} \phi_{n_i}(Q_i), \tag{25}$$

where $Q_i$ are normal mode stretches and $n_i$ are the vibrational quantum numbers of the harmonic oscillators with frequencies $\omega_i$, given in Table I.

To describe the internal motion of the dissociative state, we use harmonic oscillator functions with $\rho$-dependent frequencies and bond lengths given by Eqs. (20-22). The translational wave function describing relative motion is the solution of Eq. (17), which contains the coupling between internal and relative motions in the effective potential of Eq. (18). This approach for the D state surface differs from the usual procedures of approximating this region of the PES by a linear or exponential function [19-20], and neglecting the $\rho$-dependence of the vibrational energy contributions to $U_{eff}$. The latter approaches result in analytical forms (Airy or Bessel functions) for the translational wave function. In the present method both terms of $U_{eff}(\rho, q^A, q^B)$ can be obtained from MCHF calculations. As will be discussed below, the *ab initio* MCHF data points are used to obtain an exponential fit for the dis-

sociative state electronic PES in the crossing point region. The calculated vibrational energy is added to the electronic potential resulting in $U_{eff}(\rho, q^A, q^B)$, from which the translational wave function, $\phi_{rel}(\rho, q^A, q^B)$, is calculated using standard numerical methods [45].

The nuclear wave functions of the quasidiscrete and dissociative states are conveniently expressed in terms of their respective sets of normal coordinates. However, evaluation of the FC integral of Eq. (24) is computationally simpler if the nuclear wave functions are expressed in a single coordinate system. For this purpose, we choose the internal coordinates $(\rho, q^A, q^B)$. The normal modes of the quasidiscrete state can be expressed as

$$Q_i = a_i \tau_A + b_i \tau_B + c_i \rho' \qquad i = \{1,2,3\}, \tag{26}$$

where

$$\begin{aligned} \tau_A &= q^A - q_o^A \\ \tau_B &= q^B - q_o^B \\ \rho' &= \rho - \rho_o \end{aligned} \tag{27}$$

represent the deviations from the equilibrium geometry. Similarly, the normal mode functions of the dissociative state can be written

$$\begin{gathered} Q_Z = a_Z(\rho)\,[\tau_A - \delta q^A(\rho)] + b_Z(\rho)\,[\tau_B - \delta q^B(\rho)] + c_Z(\rho)\,\rho' \\ Z \equiv \{A,B\}, \end{gathered} \tag{28}$$

where the difference between the equilibrium bond lengths of the quasidiscrete and dissociative states are given by

$$\begin{aligned} \delta q^A(\rho) &= q_o^A - q_{oD}^A(\rho) \\ \delta q^B(\rho) &= q_o^B - q_{oD}^B(\rho). \end{aligned} \tag{29}$$

In this coordinate system the multidimensional FC overlap of Eq. (24) can be written

$$H'_{D\leftarrow Q} \sim \int \Big[ \int \phi_{n_1}(\tau_A, \tau_B, \rho')\, \phi_{n_2}(\tau_A, \tau_B, \rho')\, \phi_{n_3}(\tau_A, \tau_B, \rho') \\ \phi_{n_A}(\tau_A, \tau_B, \rho')\, \phi_{n_B}(\tau_A, \tau_B, \rho')\, d\tau_A\, d\tau_B \Big] \phi_{rel}(\rho')\, d\rho'. \tag{30}$$

Integrations over $\tau_A$ and $\tau_B$ can be done analytically resulting in a one-dimensional integral of the form

$$H'_{D\leftarrow Q} \sim \int \phi_{vib}(\rho')\, \phi_{rel}(\rho')\, d\rho', \tag{31}$$

where $\phi_{vib}(\rho')$ is an effective vibrational wave function of the form

$$\phi_{vib}(\rho') \sim F(\rho') \exp[-(\rho' - \delta\rho)^2/c^2]. \tag{32}$$

Here F is a complicated function of the vibrational frequencies, the coordinate transformation coefficients, the vibrational quantum numbers, the changes in the equilibrium bond lengths, and $\rho'$. The explicit form of $\phi_{vib}$ is given in Appendix D. The gaussian factor is centered at $\rho_o + \delta\rho$ and has width c. The shift $\delta\rho$ results from the changes in the equilibrium bond lengths of the CN fragments in the Q and D states. Final integration of Eq. (31) is performed numerically [45]. The transition probability in Eq. (1) is obtained from the product of the square of the transition matrix element, $H_{D\leftarrow Q}$, multiplied by the final density of states, $\rho_E$. The one-dimensional final density of states is proportional to the inverse of the asymptotic momentum [33].

Because $H'_{D\leftarrow Q}$ is explicitly a function of the vibrational quantum numbers, it yields state-to-state transition probabilities and thus final-state vibrational energy distributions. It has been shown previously [13] that Eqs. (31) and (32) can lead to inverted vibrational distributions. The possibility of an inverted distribution arises from the fact that for low vibrational levels and hence large relative kinetic energy the translational wave function is a highly oscillatory function which can lead to small nuclear overlap and

transition probabilities. However, transition probabilies to high vibrational states can also be reduced because of a larger effective potential which displaces the classical turning point further from the center of the effective vibrational wave function. The latter favors a noninverted distribution. In general, the PVDs will depend on these competing factors which ultimately are determined by the PESs and the $\rho$-dependence of the vibrational energy.

*Vibrational Distributions*

Figure 5 shows a section of the diabatic potential energy surfaces from the *ab initio* STO-3G MCHF calculations of the Q and D states. The points of the D state curve define the minimum energy path that satisfies the conditions of Eqs. (16) and (C3). The corresponding points of the Q surface were calculated at the same nuclear geometries. The crossing point of the two curves occurs near $\rho = 2.95$ Å corresponding to 8.9 eV. The main contributions to the FC overlap will come from the region near the crossing point. It is reasonable to approximate the repulsive electronic PES by an exponential of the form

$$U(\rho, q_o^A(\rho), q_o^B(\rho)) = U_\infty + A \exp(-\gamma\, \rho'). \tag{33}$$

Others [17,20,25] have employed similar exponential forms for a D state PES, where the parameters A and $\gamma$ were determined from experimental data or electronic structure calculations. This results in a Bessel function for the translational wave function simplifying the $H'_{D\leftarrow Q}$ integral. The *ab initio* calculations yield $A = 2.4 \cdot 10^9$ cm$^{-1}$ and $\gamma = 3.95$ Å$^{-1}$ in Eq (33).

The magnitudes of the transition probabilities and PVDs will be sensitive to the classical turning points of the D state PES. The effective vibrational wave function is centered near the Q state minimum, $\rho_o$. The translational

wave function will not have appreciable amplitude until the classical turning point, $\rho_{tp}$. Inspection of Figure 5 indicates that $\rho_o = 2.66$Å and $\rho_{tp} = 3.15$Å at 164 nm. The STO-3G PESs yield very small transition probability with overlap resulting mainly from the exponentially decreasing tails of the nuclear wave functions in the classically forbidden region.

The computed transition probabilities (and $\rho_{tp}$) are found to be considerably more sensitive to the PES parameter $\gamma$ than to the preexponential factor A of Eq. (33). Variations in A displace the D state curve without changing its shape; whereas, changes in $\gamma$ affect the curvature. For example, at 164 nm, a 20% decrease in A from $2.4 \cdot 10^9$ to $1.82 \cdot 10^9$ cm$^{-1}$ decreases $\rho_{tp}$ by 0.06 Å (2% change); however, a 20% increase in $\gamma$ from 3.95 to 4.74 Å$^{-1}$ decreases $\rho_{tp}$ by 0.54 Å (17% change) which significantly alters the computed PVDs.

The 164 nm photon energy is only 0.26 eV above the ground vibrational level of $C_2N_2(\tilde{C}\ ^1\Pi_u)$. Because predissociation is experimentally observed at this energy, we expect the crossing point to actually occur at lower energy and a smaller interfragment distance than depicted by the calculated STO-3G MCHF PESs. Given the sensitivity of computed PVDs to the D state electronic PES parameters, we have carried out the analysis using the *ab initio* STO-3G value for the less sensitive pre-exponential factor A leaving the exponential constant $\gamma$ to be determined from a fit to the experimental data. Extended basis set calculations (DZP level) are in progress. Preliminary results indicate a lower D state PES as expected.

**CN(X $^2\Sigma^+$) PVDs.** The experiments of Miller et al. and Jackson [21,23-24] were done at three photon wavelengths separated by $\sim$ 2100 cm$^{-1}$, the vibrational frequency of the symmetric CN stretch. The lowest wavelength,

164 nm, is also about 2100 $cm^{-1}$ above the ground vibrational level of $C_2N_2(\tilde{C}\ ^1\Pi_u)$. Thus, it is reasonable to assume that the initial state reached at 164 nm is (1,0,0) corresponding to one vibrational quantum in the symmetric CN stretch. Here we label the initial Q state by ($\nu_1$, $\nu_2$, $\nu_3$) where $\nu_1$ refers to the vibrational quantum number of the symmetric CN stretch, $\nu_2$ identifies the CC stretch, and $\nu_3$ corresponds to the asymmetric CN stretch. On this basis the symmetric CN stretch is excited at 158.7nm with one additional quantum (2,0,0), and two more quanta (3,0,0) at 153.6nm. Because Miller et al. report only the CN(X $^2\Sigma^+$) vibrational populations at these wavelengths, our computed results, which only consider the single surface predissociation of channel II, can be directly compared to experiment.

Figure 6 compares computed CN(X $^2\Sigma^+$) PVDs to the measurements of Miller et al. Good qualitative agreement is obtained for $A = 2.4 \cdot 10^9$ $cm^{-1}$ and $\gamma \approx 4.64$–$4.88$ $Å^{-1}$ of Eq. (33). These values indicate a more repulsive surface in the FC region to obtain increased nuclear overlap than that obtained from the minimum basis set MCHF calculations. The effective potential curves (Eq. (18)) for transitions at 164 nm to several final states are shown in Figure 7. The dips in the effective potential at 3.2 Å reflect the $\rho$-dependence of the frequencies in the vibrational energy contribution (see Fig. 4). We had sought a single $\gamma$ to satisfy the experimental data, but found instead a small range of values that provided agreement with the CN(X $^2\Sigma^+$) data. These findings support our expectation of a crossing point lower in energy and at a smaller interfragment separation as shown in Fig. 7.

In a recent study, Eros et. al. [46], reported 133 kcal for the dissociation energy of ground state $C_2N_2(\tilde{X}\ ^1\Sigma_g^+)$ - 5 kcal larger than the previously

accepted value. This difference ( $\sim$ 1750 $cm^{-1}$) changes the number of energeticially accessible fragment vibrational channels and hence the calculated distributions. The effect of this increased binding is to raise the effective potential, resulting in less nuclear overlap and smaller transition probabilties. Similar qualitative agreement between calculated and experimental CN(X $^2\Sigma^+$) vibrational distributions is obtained with this increased dissociation energy but it requires a slightly larger $\gamma$, i.e., $4.72<\gamma<5.02$ $\AA^{-1}$ to compensate for the larger binding.

**CN(A $^2\Pi$) PVDs.** At 157.6 nm laser energy used in the experiments of Taherian et al., channel III becomes accessible with the possibility of forming two CN(A $^2\Pi$, $\nu = 0$) fragments. We have not calculated contributions from this channel and therefore cannot make a direct comparison with experiment. Because channel III can only contribute CN(A $^2\Pi$) fragments in $\nu = 0$, however, the vibrational distribution solely from channel II should be peaked at $\nu = 2$ in order that the total distribution from both channels have the bimodal character observed by Taherian et al.

At 157.6 nm it is not clear which initial vibrational level of $C_2N_2(\tilde{C}\ ^1\Pi_u)$ is reached. A 157.6 nm photon has energy 440 $cm^{-1}$ above the (2,0,0) vibrational state and it is possible that this excess energy goes into the bending and rotational modes not considered here. With the assumption that the initial state is (2,0,0) we have estimated the contribution from channel II. No reasonable values of the exponential parameters of Eq. (33) resulted in a vibrational distribution peaked at $\nu = 2$. At all wavelengths for which the initial state contained only excitation into the symmetric CN stretch of $C_2N_2(\tilde{C}\ ^1\Pi_u)$, all PVDs had greater than 99% of the CN(A $^2\Pi$) fragments

formed in $\nu = 0$. Inclusion of contributions from channel III would only lead to poorer agreement with experiment.

The behavior of the CN(A $^2\Pi$) vibrational distributions can be explained with symmetry arguments. As discussed above, the photofragments have a supermolecule appearance in the FC region. The normal modes of the dissociative state in this region are symmetric ($\Sigma_g^+$) and asymmetric ($\Sigma_u^+$) linear combinations of localized CN bond stretches similar to those of $C_2N_2(\tilde{C}\ ^1\Pi_u)$. Orthogonality of the Hermite functions describing these normal modes yields a propensity rule for the sum of the vibrational quantum numbers of the asymmetric stretches. Their sum must be even for a nonzero transition probability. Since we assume that the quasidiscrete initial states are excitations of the symmetric CN stretch with the asymmetric CN stretch in its zero-point level, by symmetry the transition probabilty to fragment states with odd quanta in the asymmetric CN stretching mode (which asymptotically becomes the CN(A $^2\Pi$) stretch) will be small.

Okabe and Jackson [24] note that if the $C_2N_2(\tilde{X}\ ^1\Sigma_g^+)$ dissociation energy is 133 kcal, then the thermodynamic limit for the CN(A $^2\Pi$) fragment at 157.6 nm would be $\nu = 4$. According to these authors, the fact that Taherian et al. observe $\nu = 5$, coupled with the possibility of multiphoton effects, casts doubt on their analysis. Okabe and Jackson [24] state that the two experiments (Taherian et al. and Miller et al.) are in direct contradiction unless the predissociative dynamics are highly sensitive to the exact point within the absorption band excited by the laser.

**Mode Specificity.** Photodissociation dynamics offer a unique possibility for the study of internal energy redistribution in a molecule. A predissociat-

ing molecule can be prepared in different initial levels of nearly the same energy from which one can observe whether mode-specific behavior occurs. Figure 8 compares theoretical vibrational distributions obtained for different initial states at 164 nm. Our computations yield characteristically different PVDs depending on the quantum number of the Q state asymmetric CN stretch, $\nu_3$. The propensity rule described in the previous section, namely that the sum of the quantum numbers of the asymmetric stretches of the Q and D states, $\nu_3 + \nu_A$, be even for nonzero probability for the transition $(\nu_X, \nu_A) \leftarrow (\nu_1, \nu_2, \nu_3)$, accounts for this behavior. This propensity rule can be expressed

$$W_{D\leftarrow Q} = \begin{cases} W_{(\nu_X, \nu_A)\leftarrow(\nu_1, \nu_2, \nu_3)} & , \nu_3 + \nu_A \text{ even} \\ \sim 0 & , \nu_3 + \nu_A \text{ odd} \end{cases} \tag{34}$$

Here the probability of a specific D←Q transition is given by $W_{D\leftarrow Q}$ and we denote final states by $(\nu_X, \nu_A)$ where the subscripts refer to the vibrational quantum numbers of the CN(X $^2\Sigma^+$) and CN(A $^2\Pi$) stretches. The population of X-state or A-state fragments with vibrational quantum number, $\nu_X$ or $\nu_A$ can be written

$$\begin{aligned} P^X_{\nu_X\leftarrow(\nu_1, \nu_2, \nu_3)} &\sim \sum_{\nu_A} W_{(\nu_X, \nu_A)\leftarrow(\nu_1, \nu_2, \nu_3)} \\ P^A_{\nu_A\leftarrow(\nu_1, \nu_2, \nu_3)} &\sim \sum_{\nu_X} W_{(\nu_X, \nu_A)\leftarrow(\nu_1, \nu_2, \nu_3)} \ . \end{aligned} \tag{35}$$

At 164 nm there is enough energy to reach final states for which $\nu_T \equiv \nu_X + \nu_A \leq 3$. Following the propensity rule Eq. (34), for Q state (1,0,0), transitions occur to D state channels with $\nu_A$ even. On the other hand, for Q state (0,0,1), transitions occur to product channels with $\nu_A$ odd. Our results for 164 nm indicate that the transition probabilities to states with

$\nu_T \geq 2$ are negligible. Table II gives the dominant terms that contribute to the fragment populations in Eq. (35).

From Figure 8, we see that for (1,0,0), both fragments are primarily populated in their ground vibrational level. Nearly 100% of the CN(A $^2\Pi$) fragments are in $\nu_A = 0$ due to the propensity rule which does not allow transitions to product channels with $\nu_A = 1$. We can explain the PVD for the ground state CN(X $^2\Sigma^+$) fragments from the dominant terms contributing to the populations (see Table II). For product channels with larger $\nu_T$ the effective potential increases. The classical turning point will be shifted to a larger interfragment distance and, in general, away from the effective oscillator. In many cases, we would expect this shift to result in less nuclear overlap and smaller transition probabilities. From this reasoning, $W_{(0,0)\leftarrow(1,0,0)}$ would be larger than $W_{(1,0)\leftarrow(1,0,0)}$; and hence, $P^X_{0\leftarrow(1,0,0)} > P^X_{1\leftarrow(1,0,0)}$.

The effect of the propensity rule is seen much more strongly in the CN(A $^2\Pi$) PVDs. The behavior of the PVDs changes dramatically between Q (1,0,0) and Q (0,0,1). For (1,0,0), the CN(A $^2\Pi$) fragments are predominantly populated in $\nu_A = 0$, as transitions to product channels with $\nu_A = 1$ are not allowed. The opposite is true for (0,0,1), as product channels with $\nu_A = 0$ are nearly zero and A-state fragments are mostly $\nu_A = 1$, resulting in an inverted vibrational distribution. We emphasize that the propensity rule, Eq. (34), arises from the symmetry of the system in the FC region at small interfragment separations

## IV. Conclusions and Remarks

We have applied our adiabatic theory of polyatomic photodissociation to $C_2N_2(\tilde{C}\ ^1\Pi_u)$ to obtain product vibrational distributions for CN(X $^2\Sigma^+$) and

CN(A $^2\Pi$) photofragments. The theory treats type II (vibrational) predissociation as a quantum transition in a diabatic representation. Relative product vibrational distributions are obtained from the evaluation of multidimensional Franck-Condon overlap integrals. The adiabatic description of the nuclear dynamics explicitly treats final-state interactions, i.e, the coupling between the relative motion of the fragments with their internal degrees of freedom, as an integral part of the theory.

*Ab initio* MCHF calculations using a minimum basis set (STO-3G) were used to construct the diabatic electronic potential energy surfaces and to compute the geometries and force constants necessary to determine nuclear wave functions. We found a strong dependence of the dissociative state fragment bond lengths and frequencies on the interfragment distance, $\rho$. As depicted in Figure 4, our calculations show that the CN(X $^2\Sigma^+$) + CN(A $^2\Pi$) dissociative state has a supermolecule appearance for small interfragment separations, where the CN fragments are indistinguishable. There exists a large variation of CN vibrational frequencies that correlates with symmetry breaking of the CN fragments as they separate and become recognizable as CN(X $^2\Sigma^+$) and CN(A $^2\Pi$) radicals.

Qualitative agreement with experiment is obtained for relative vibrational distributions for CN(X $^2\Sigma^+$) at 164, 158.7, and 153.6 nm. These results were obtained assuming the initial state of the precursor $C_2N_2(\tilde{C}\ ^1\Pi_u)$ system to include only excitation of the symmetric CN stretching mode. At 157.6 nm the initial $C_2N_2(\tilde{C}\ ^1\Pi_u)$ vibrational state could not be ascertained from the present study. Direct comparison with experiment would entail inclusion of the product channel corresponding to two CN(A $^2\Pi$) fragments. However, at

this photon energy, the experimental bimodal distribution obtained for CN(A $^2\Pi$) could not be reproduced. It is possible that bending vibrations or rotations are important which must await three-dimensional studies in progress.

Another result of our analysis is the occurrence of mode specificity. Computed product vibrational distributions for $C_2N_2(\tilde{C}\ ^1\Pi_u)$ prepared with quanta solely in the symmetric CN stretching mode $\nu_1$ differ from those with the same number of quanta solely in the asymmetric mode $\nu_3$. A propensity rule is found for $\sigma \equiv \nu_3 + \nu_{A\ ^2\Pi}$: for $\sigma$ odd, the transition probabilty will be small or nearly zero. This propensity rule results from symmetry restrictions arising from the parity of normal modes functions for the Franck-Condon-type integrals.

## Appendix A: General Expression For The Transition Probability [41]

One can write the total Hamiltonian

$$\hat{H} = \hat{H}_o + \hat{V}(t)\,. \tag{A1}$$

The wave function can be expressed in terms of the eigenfuctions, $\psi_n$, and eigenvalues, $E_n$, of $\hat{H}_o$

$$\Psi = \sum_n a_n(t)\ \psi_n\ e^{-iE_n t/\hbar}\,. \tag{A2}$$

If the system is initially in a stationary state with energy $E_m$, the probability of being in a stationary state with energy $E_n$ after the interaction is given by the absolute square of the coefficients $a_{nm}(t)$

$$\omega_{nm}(t) = \left|a_{nm}(t)\right|^2\,. \tag{A3}$$

The solution of $a_{nm}$ is an infinite series which can be expressed in terms of transition matrix, $<n \mid \hat{T} \mid m>$, where

$$<n \mid \hat{T} \mid m> = <n \mid \hat{V} \mid m> + \sum_{f} \frac{<n \mid \hat{V} \mid f><f \mid \hat{V} \mid m>}{E_m - E_f + i\eta} + \sum_{f,f'} \frac{<n \mid \hat{V} \mid f><f \mid \hat{V} \mid f'><f' \mid \hat{V} \mid m>}{(E_m - E_f + i\eta)(E_m - E_{f'} + i\eta)} + \cdots \quad . \tag{A4}$$

If $\hat{V}(t) = \hat{V}$, then transitions can only occur between states of equal energy. The general expression for the transition probability per unit time from initial state $\mid m>$ to a final state $\mid n>$ can be expressed as

$$W_{nm} = \frac{2\pi}{\hbar} \delta(E_n - E_m) \left| <n \mid \hat{T} \mid m> \right|^2 . \tag{A5}$$

In first-order $\hat{T} = \hat{V}$ resulting in the well-known golden rule expression of Eq. (1). The higher order terms correspond to transitions to virtual electronic states. From Eq. (A4) one can see that these higher-order terms contain products of Franck-Condon factors resulting in additional orders of smallness and serve as a check of the applicability of Eq. (1). Based on Eq. (A4) one can calculate higher-order terms to obtain a desired accuracy. We note here that our approach differs from those based on scattering theory [36,38] which lead to only a single Franck-Condon factor.

## Appendix B: Wave Functions in the Adiabatic Limits

In this appendix we report the solutions for the nuclear Schrödinger equation in the two adiabatic limits following a similar analysis presented earlier [1e,1-4].

Case (i): *Fast Translational Motion* , $\alpha \equiv \frac{\epsilon_{rel}}{\epsilon_{int}} >> 1$

In this limit we can use the clamped translational function approximation [1-4] and obtain for the D state nuclear wave function the product function,

$$\tilde{\phi}_D(\rho, q^A, q^B) = \phi_{rel}(\rho, q_o^{A'}, q_o^{B'})\, \phi_{int}(q^A, q^B). \tag{B1}$$

The wave function describing relative motion, $\phi_{rel}$, is the solution of

$$\left[-\frac{1}{2\mu}\frac{\partial^2}{\partial\rho^2} + U(\rho, q_o^{A'}, q_o^{B'})\right]\phi_{rel}(\rho, q_o^{A'}, q_o^{B'}) = E(q_o^{A'}, q_o^{B'})\, \phi_{rel}(\rho, q_o^{A'}, q_o^{B'}). \tag{B2}$$

In the harmonic approximation, $\phi_{int}$ is given by

$$\phi_{int}(q_A, q^B) = \phi_{n_A}^{A}(Q_A(\tau_A^i, \tau_B^i))\, \phi_{n_B}^{B}(Q_B(\tau_A^i, \tau_B^i)), \tag{B3}$$

where

$$\phi_{n_Z}^{Z}(Q_Z(\tau_A^i, \tau_B^i)) = \left(\frac{\omega_Z^i}{\pi\hbar}\right)^{1/4} \frac{1}{\sqrt{2^{n_Z}\, n_Z!}} \exp\left(-\frac{\omega_Z^i\, Q_Z^2(\tau_A^i, \tau_B^i)}{2\hbar}\right) \cdot H_Z\left(Q_Z(\tau_A^i, \tau_B^i)\sqrt{\frac{\omega_Z^i}{\hbar}}\right). \tag{B4}$$

Here, $Q_z$ are normal coordinates, which in this limit are the asymptotic bond stretches of the product fragments. The $\omega_Z^i$ are vibrational frequencies, $Z \equiv \{A,B\}$ refers to product fragments, and $\tau_Z^i$ are given by

$$\tau_Z^i = q^Z - q_o^{Z'}. \tag{B5}$$

It can be shown [14] that in this limit the vibrational frequencies and equilibrium bond lengths are constants and can be well approximated by their asymptotic noninteracting-fragment values, $\omega_{asy}$ and $q_{asy}$.

Case (ii): *Slow Translational Motion* , $\alpha << 1$

In this limit the wave function is also separable into two functions of the form

$$\tilde{\phi}_D(\rho, q^A, q^B) = \phi_{rel}(\rho)\, \phi_{int}(q^A, q^B; \rho). \tag{B6}$$

Here the wave function describing the internal motion depends parametrically on the interfragment separation $\rho$ and can be written

$$\phi_{int}(q^A, q^B; \rho) = \phi^A_{n_A}(Q_A(\tau^{ii}_A(\rho), \tau^{ii}_B(\rho); \rho))\, \phi^B_{n_B}(Q_B(\tau^{ii}_A(\rho), \tau^{ii}_B(\rho); \rho)). \tag{B7}$$

Again in the harmonic approximation,

$$\phi^Z_{n_Z}(Q_Z(\tau^{ii}_A(\rho), \tau^{ii}_B(\rho); \rho)) = \left(\frac{\omega^{ii}_Z(\rho)}{\pi\hbar}\right)^{1/4} \frac{1}{\sqrt{2^{n_Z}\, n_Z!}}$$
$$\cdot \exp\left(-\frac{\omega^{ii}_Z(\rho)\, Q^2_Z(\tau^{ii}_A(\rho), \tau^{ii}_B(\rho); \rho)}{2\hbar}\right) H_Z\left(Q_Z(\tau^{ii}_A(\rho), \tau^{ii}_B(\rho); \rho)\sqrt{\frac{\omega^{ii}_Z(\rho)}{\hbar}}\right). \tag{B8}$$

As above, $Q_Z$ are normal coordinates, which asymptotically become the individual bond stretches of each product fragment (see Section III). The $\omega^{ii}_Z(\rho)$ are vibrational frequencies of the fragments, and $\tau^{ii}_Z(\rho)$ are given by

$$\tau^{ii}_Z(\rho) = q^Z - q_o^{Z^{ii}}(\rho). \tag{B9}$$

The wave function $\phi_{rel}$ is obtained by solving

$$\left[-\frac{1}{2\mu}\frac{\partial^2}{\partial\rho^2} + U_{eff}(\rho)\right]\phi_{rel}(\rho) = E\, \phi_{rel}(\rho), \tag{B10}$$

where the effective potential $U_{eff}$ is

$$U_{eff}(\rho) = U(\rho, q_o^{A^{ii}}(\rho), q_o^{B^{ii}}(\rho)) + (n_A + 1/2)\hbar\,\omega^{ii}_A(\rho) + (n + 1/2)\hbar\,\omega^{ii}_B(\rho). \tag{B11}$$

One notes that in this limit, the vibrational frequencies and equilibrium bond lengths are functions of $\rho$ and differ quite significantly from their asymptotic values (see Figure 4).

*Intermediate Cases* , $\alpha \approx 1$

The general form of $\tilde{\phi}_D$ for arbitrary $\alpha$ given by Eqs. (14,17-22) results from comparison of the solutions for the two limiting cases given above. In both limits the total nuclear wave function is expressed as a product of two functions (see Eqs. (B1) and (B6)). Moreover, the structure of the corresponding functions for each case is very similar (cf. (B3) and (B7), (B4) and (B8), (B2) and (B10), (B5) and (B9)). One notes that the limiting cases differ only in the explicit form of the vibrational frequencies and equilibrium bond lengths. For $\alpha >> 1$, the frequencies and bond lengths are functions of $\rho$ (see (B8) and (B9)); whereas, the case $\alpha << 1$ is characterized by constant values of these quantities. Therefore, it appears reasonable to conclude that a continuous change occurs from the limit $\alpha << 1$ to the opposite case, accompanied by a change in the $\rho$-dependence of the vibrational frequencies and equilibrium bond lengths. This transition is describable by the interpolation expression of Eq. (22).

## Appendix C: Optimization On The Minimum Energy Path

We seek the minimum energy molecular geometry for a fixed interfragment distance $\rho$. Employing the method of Lagrange multipliers, we introduce the function $G \equiv U + \lambda\rho$ for which we want to satisfy

$$dG = dU + \lambda d\rho = 0, \tag{C1}$$

where U is the electronic potential depending on the nuclear positions and $\lambda$ is a constant. For a linear tetra-atomic, choosing the molecular axis to be along the Z axis,

$$\rho = \frac{m_3Z_3 + m_4Z_4}{m_3 + m_4} - \frac{m_1Z_1 + m_2Z_2}{m_1 + m_2}. \tag{C2}$$

Here $Z_i$ is the Z-coordinate of the ith atom. For $C_2N_2$, $m_1=m_4\equiv m_N$, and $m_2=m_3\equiv m_C$. Substituting (C2) in (C1) results in the following condition for the gradients of the atoms on the minimum energy path

$$\frac{\partial U}{\partial Z_1} : \frac{\partial U}{\partial Z_2} : \frac{\partial U}{\partial Z_3} : \frac{\partial U}{\partial Z_4} = m_N : m_C : -m_C : -m_N. \tag{C3}$$

Geometries and force constants (i.e., second derivatives of the energy with respect to nuclear coordinate) along the reaction path were calculated using the minimum basis MC10 wave function for the dissociative state (see Sec. III). Because these geometries are not stationary points of the potential energy surface, the usual procedure of diagonalizing the force constant matrix to obtain 3N-5 (linear molecule) normal modes and frequencies is not valid. The variable $\rho$ corresponds to unbounded relative motion of the photofragments. We can employ the reaction path Hamiltonian method of Miller, Handy, and Adams [47] to obtain the frequencies of the normal coordinates orthogonal to the reaction path. In this procedure one projects out the reaction path from the matrix of second derivatives of the energy w.r.t. nuclear coordinates to obtain the projected force constant matrix

$$K^P = (1-P)\cdot K\cdot(1-P), \tag{C4}$$

where K and P have dimensions $3N\times 3N$ and are given by

$$\begin{aligned} K_{i,j} &= \frac{\partial^2 U}{\partial Z_i \partial Z_j} \\ P_{i,j} &= \hat{L}_i\cdot\hat{L}_j. \end{aligned} \tag{C5}$$

Here $\hat{L}$ is a 3N-dimensional unit vector which defines the direction of the reac-

tion path and the subscripts i and j label nuclei. Diagonalization of $K^P$ results in 3N-6 nonzero eigenvalues corresponding to the frequencies of the normal coordinates orthogonal to the reaction path. The 6 null eigenvalues correspond to the infinitesimal translations(3) and rotations(2) of an N-atom linear molecule, and motion along the reaction path. For $C_2N_2$ constrained to be linear, the gradients obey the simple relationship given by Eq. (C3); the unit vector $\hat{L}$ is constant for all values of $\rho$ and is given by

$$\begin{aligned} \hat{L}_1 &= \frac{m_N}{M}\,\hat{Z}_1 \\ \hat{L}_2 &= \frac{m_C}{M}\,\hat{Z}_2 \\ \hat{L}_3 &= -\frac{m_C}{M}\,\hat{Z}_3 \\ \hat{L}_4 &= -\frac{m_N}{M}\,\hat{Z}_4 \end{aligned} \tag{C6}$$

where $M = \sqrt{2(m_N^2 + m_C^2)}$ .

## Appendix D: The Effective Vibrational Wave Function

The transition matrix element, Eq. (30), can be rewritten

$$H_{D\leftarrow Q} = \int \left[ \int \prod_{i=1}^{5} \phi_{n_i}(Q_i)\, d\tau_A\, d\tau_B \right] \phi_{rel}(\rho')\, d\rho'. \tag{D1}$$

Here, i={1,2,3} refers to the symmetric CN, CC, and asymmetric CN stretching modes of the quasidiscrete state and i={4,5} refers to the dissociative state symmetric CN and asymmetric CN stretches which asymptotically correlate to CN(X $^2\Sigma^+$) and CN(A $^2\Pi$) localized bond stretches. The normal coordinates can also be expressed in terms of internal coordinates similar to Eqs. (26-29)

$$Q_i = a_i(\tau_A - \delta q_i^A) + b_i(\tau_B - \delta q_i^B) + c_i\rho' \tag{D2}$$

The harmonic oscillator functions have the usual form

$$\phi_{n_i}(Q_i) = \left(\frac{\omega_i}{\pi\hbar}\right)^{1/4} \left[2^{n_i} n_i!\right]^{-1/2} \exp\left(\frac{\omega_i Q_i^2}{2\hbar}\right) H_{n_i}\left(Q_i\sqrt{\frac{\omega_i}{\hbar}}\right). \tag{D3}$$

For the quasidiscrete state $i=\{1,2,3\}$ the transformation coefficients ($a_i$, $b_i$, $c_i$), vibrational frequencies ($\omega_i$), and changes in equilibrium bond lengths ($\delta q_i = 0$) are constants. However, for the dissociative state $i=\{4,5\}$, they depend on both $\rho$ and $\alpha$ as given by Eqs. (22,28,29).

The effective vibrational wave function is the term enclosed by brackets in Eq. (D1). Substituting Eqs. (D2) and (D3) in Eq. (D1) and employing the generating function for Hermite polynomials

$$H_{n_i}(x_i) = \left(\frac{\partial}{\partial t_i}\right)^{n_i} \exp\left(-t_i^2 + 2\, x_i\, t_i\right)\Big|_{t_i = 0}, \tag{D4}$$

one can integrate over the internal coordinates analytically resulting in the following expression

$$\phi_{vib}(\rho') = \left(\frac{\prod_{i=1}^{5}\omega_i}{\pi^5\hbar^5}\right)^{1/4} \left[2^{(n_1+n_2+n_3+n_4+n_5)} \cdot \prod_{i=1}^{5} n_i!\right]^{-1/2} \frac{\pi^2}{A \cdot B^1} \prod_{i=1}^{5}\left(\frac{\partial}{\partial t_i}\right)^{n_i} \tag{D5}$$

$$\cdot \exp\left[\frac{G^2}{4\,A} + \frac{H_1^2}{4\,B_1} + \frac{J_1^2}{4\,C_1} - K\right] \exp\left[-C_1\left(\rho' + \frac{J_1}{2C_1}\right)^2\right]\Big|_{\text{all } t_i\text{'s} = 0}$$

where

$$A = \sum_{i=1}^{5} \frac{a_i^2\,\omega_i}{2\,\hbar}$$

$$B = \sum_{i=1}^{5} \frac{b_i^2\, \omega_i}{2\, \hbar}$$

$$C = \sum_{i=1}^{5} \frac{c_i^2\, \omega_i}{2\, \hbar}$$

$$D = \sum_{i=1}^{5} \frac{a_i\, b_i\, \omega_i}{\hbar}$$

$$E = \sum_{i=1}^{5} \frac{a_i\, c_i\, \omega_i}{\hbar}$$

$$F = \sum_{i=1}^{5} \frac{b_i\, c_i\, \omega_i}{\hbar}$$

$$G = -\left[ 2 \sum_{i=1}^{5} a_i \sqrt{\frac{\omega_i}{\hbar}}\, t_i + \sum_{i=1}^{5} \frac{\omega_i}{\hbar} \left( a_i^2\, \delta q_i^A + a_i\, b_i\, \delta q_i^B \right) \right]$$

$$H = -\left[ 2 \sum_{i=1}^{5} b_i \sqrt{\frac{\omega_i}{\hbar}}\, t_i + \sum_{i=1}^{5} \frac{\omega_i}{\hbar} \left( a_i\, b_i\, \delta q_i^A + b_i^2\, \delta q_i^B \right) \right]$$

$$J = -\left[ 2 \sum_{i=1}^{5} c_i \sqrt{\frac{\omega_i}{\hbar}}\, t_i + \sum_{i=1}^{5} \frac{\omega_i}{\hbar} \left( a_i\, c_i\, \delta q_i^A + a_i\, b_i\, \delta q_i^B \right) \right]$$

$$K = \sum_{i=1}^{5} t_i^2 + \sum_{i=1}^{5} \frac{\omega_i}{2\, \hbar} \left( a_i^2\, \delta q_i^{A^2} + b_i^2\, \delta q_i^{B^2} \right)$$

$$+ 2 \sum_{i=1}^{5} \sqrt{\frac{\omega_i}{\hbar}} \left( a_i\, \delta q_i^A + b_i\, \delta q_i^B \right) t_i + \sum_{i=1}^{5} \frac{\omega_i}{\hbar} \left( a_i\, b_i\, \delta q_i^A\, \delta q_i^B \right)$$

$$B_1 = B - \frac{D^2}{4\, A}$$

$$H_1 = H - \frac{D\, G}{2\, A}$$

$$F_1 = F - \frac{D\, E}{2\, A}$$

$$C_1 = C - \frac{E^2}{4\, A} - \frac{F_1^2}{4\, B_1}$$

$$J_1 = J - \frac{G\,E}{2\,A} - \frac{F_1\,H_1}{2\,B_1}$$

Note that G, $H_1$, $J_1$, and K all are functions of the dummy variables $t_i$ which arise from the generating function of Eq. (D4) of the Hermite polynomials. The effective vibrational wave function for a particular vibrational transtion $(n_1, n_2, n_3) \rightarrow (n_4, n_5)$ can be obtained from differentiating Eq. (D5) w.r.t. $t_i$. The resulting expression has the form of Eq. (32).

## References


1. See, for example, (a) S. A. Rice, in *Excited States,* (E. C. Lim, Ed.), **vol. 2**, Academic Press, New York, 1975, p. 111; (b) K. F. Freed and Y. B. Band, in *Excited States,* (E. C. Lim, Ed.), **vol. 3**, Academic Press, New York, 1977, p. 109; (c) W. F. Gelbart, Ann. Rev. Phys. Chem. **28**, 323 (1977); (d) M. Shapiro and R. Bersohn, Ann. Rev. Phys. Chem. **33**, 409 (1982); (e) V. Z. Kresin and W. A. Lester, Jr., in *Advances in Photochemistry,* (Volman, Gollnick, and Hammond, Eds.), **vol. 13**, John Wiley and Sons, Inc., New York, 1986, p. 95. Also, see references within.

2. E. Segev and M. Shapiro, J. Chem. Phys. **77**, 5604 (1982).

3. Y. Band, K. Freed, and D. Kouri, J. Chem. Phys. **74**, 4380 (1981).

4. (a) R. W. Heather and J. C. Light, J. Chem. Phys. **78**, 5513 (1983); **79**, 147 (1983).

5. K. Takatsuka and M. Gordon, J. Chem. Phys. **74**, 5718 (1981).

6. R. W. Numrich and K. G. Kay, J. Chem. Phys. **70**, 4343 (1979).

7. D. C. Clary, J. Chem. Phys. **84**, 4288 (1986).

8. (a) K. Kulander and J. C. Light, J. Chem. Phys. **85**, 1938 (1986); (b) **73**, 4337 (1980);

9. C. E. Caplan and M. S. Child, Mol. Phys. **23**, 249 (1972).

10. (a) Y. B. Band and K. F. Freed, J. Chem. Phys. **63**, 3382 (1975); (b) J. Chem. Phys. **67**, 1462 (1977).

11. M. Berry, Chem. Phys. Lett. **29**, 329 (1974).

12. V. Z. Kresin and W. A. Lester, Jr., Int. J. Quantum Chem., Symp. **15**, 703 (1981).

13. V. Z. Kresin and W. A. Lester, Jr., Chem. Phys. Lett. **87**, 392 (1982).

14. V. Z. Kresin and W. A. Lester, Jr., J. Phys. Chem. **86**, 2182 (1982).

15. R. T. Pack, J. Chem. Phys. **65**, 4765 (1976).

16. S. Lee and E. Heller, J. Chem. Phys. **76**, 3035 (1982).

17. J. A. Beswick, M. Shapiro, and R. Sharon, J. Chem. Phys. **67**, 4045 (1977).

18. Y. B. Band and K. F. Freed, J. Chem. Phys. **64**, 4329 (1976).

19. Y. B. Band and K. F. Freed, Chem. Phys. Lett. **28**, 328 (1974).

20. (a) O. Atabeck, J. A. Beswick, R. Lefebvre, S. Mukamel, and J. Jortner, J. Chem. Phys. **65**, 4035 (1976); (b) S. Miret-Artes, G. Delgado-Barrio, O. Atabek, and J. A. Beswick, Chem. Phys. Lett. **98**, 554 (1983).

21. G. Miller, W. M. Jackson, and J. Halpern, J. Chem. Phys. **71**, 4025 (1979).

22. M. Taherian and T. Slanger, J. Chem. Phys. **81**, 3814 (1984).

23. W. M. Jackson, J. Photochem. **17**, 509 (1981).

24. W. M. Jackson and H. Okabe, in *Advances in Photochemistry,* (Volman, Gollnick, and Hammond, Eds.), **vol. 13**, John Wiley and Sons, Inc., New York, 1986, p. 1.

25. J. A. Beswick and M. Horani, Chem. Phys. Lett. **78**, 4 (1981).

26. K. C. Kulander, Chem. Phys. Lett. **103**, 373 (1984).

27. T. O'Malley, Phys. Rev. **152**, 98 (1967).

28. F. T. Smith, Phys. Rev. **179**, 111 (1969).

29. S. Mukamel and J. Ross, J. Chem. Phys. **66**, 3759 (1977).

30. (a) B. C. Garrett, and D. G. Truhlar, in *Theoretical Chemistry: Advances and Perspectives,* (D. Henderson, ed.), **vol. 6a**, Academic Press, Inc., New York, 1981, p. 1; (b) C. A. Mead and D. G. Truhlar, J. Chem. Phys. **77**, 6090 (1982).

31. F. Rebentrost, in *Theoretical Chemistry: Advances and Perspectives,* (D. Henderson, ed.), **vol. 6b**, Academic Press, Inc., New York, 1981, p. 1.

32. G. Herzberg, *Molecular Spectra and Molecular Structure I. Spectra of Diatomic Molecules,* Van Nostrand Reinhold Co., New York, 1950.

33. See for example, L. Landau and E. Lifshitz, *Quantum Mechanics,* Pergamon Press, New York, 1976.

34. V. Z. Kresin, W. A. Lester, Jr., M. Dupuis, and C. E. Dateo, Int. J. Quantum Chem., Symp. **18**, 691 (1984).

35. V. Z. Kresin and W. A. Lester, Jr., Chem. Phys. **90**, 335 (1984).

36. (a) G. Schatz and J. Ross, J. Chem. Phys. **66**, 1021 (1977); (b) **66**, 1037 (1977); (c) **66**, 2943 (1977).

37. K. Fung and K. Freed, Chem. Phys. **30**, 249, (1978).

38. (a) C. Vila, D. Zvijac, and J. Ross, J. Chem. Phys. **70**, 2414 (1979); (b) **70**, 5362 (1979).

39. U. Halvee and M. Shapiro, J. Chem. Phys. **64**, 2836 (1976).

40. J. Bardeen, Phys. Rev. Lett. **6**, 57 (1961).

41. See for example, A. Davydov, *Quantum Mechanics,* Pergamon Press, Oxford, 1976.

42. C. E. Dateo, M. Dupuis, and W. A. Lester, Jr., J. Chem. Phys. **83**, 265 (1985).

43. R. E. Connors, J. L. Roebber, and K. Weiss, J. Chem. Phys. **60**, 5011 (1974).

44. G. Herzberg, *Molecular Spectra and Molecular Structure III. Electronic Spectra of Polyatomic Molecules,* Van Nostrand Reinhold Co., New York, 1966.

45. The translational wave functions were calculated using the computer code TDELAY, written by R. J. LeRoy, University of Waterloo Chem. Phys. Res. Reports, CP-107 (1978).

46. D. Eros, M. Gurnick, and J. D. McDonald, J. Chem. Phys. **81**, 5552 (1984).

47. W. H. Miller, N. C. Handy, and J. E. Adams, J. Chem. Phys. **72**, 99 (1980).

**Table I. Computed Properties of $C_2N_2$ and CN**

| State | Property | Calculated | Experimental |
|---|---|---|---|
| $C_2N_2(\tilde{C}\ ^1\Pi_u)$ | R(CC) | 1.308 Å | -- |
| | R(CN) | 1.252 Å | -- |
| | $\nu_1$ (sym CN) | 2082 $cm^{-1}$ | 2100 $cm^{-1}$[a] |
| | $\nu_2$ (CC) | 896 $cm^{-1}$ | -- |
| | $\nu_3$ (asym CN) | 1726 $cm^{-1}$ | -- |
| | $T_e(\tilde{C}\ ^1\Pi_u \leftarrow \tilde{X}\ ^1\Sigma_g^+)$ | 8.64 eV | 7.30 eV[a] |
| CN(A $^2\Pi$) | r(CN) | 1.2983 Å | 1.2327 Å[b] |
| | $\nu_A$ | 1716 $cm^{-1}$ | 1814 $cm^{-1}$[b] |
| | $T_e(A^2\Pi \leftarrow X^2\Sigma^+)$ | 1.53 eV | 1.146 eV[b] |
| CN(X $^2\Sigma^+$) | r(CN) | 1.2087 Å | 1.1718 Å[b] |
| | $\nu_X$ | 2101 $cm^{-1}$ | 2069 $cm^{-1}$[b] |

[a]Reference 43
[b]Reference 44

**Table II. Dominant Terms for the CN(X $^2\Sigma^+$) and CN(A $^2\Pi$) Populations at 164 nm**

| | Q (1,0,0) | Q (0,0,1) |
|---|---|---|
| $P^X_{0\leftarrow Q}$ | $W_{(0,0)\leftarrow(1,0,0)}$ | $W_{(0,1)\leftarrow(0,0,1)}$ |
| $P^X_{1\leftarrow Q}$ | $W_{(1,0)\leftarrow(1,0,0)}$ | $\sim 0$ |
| $P^X_{2\leftarrow Q}$ | $\sim 0$ | $\sim 0$ |
| $P^A_{0\leftarrow Q}$ | $W_{(0,0)\leftarrow(1,0,0)} + W_{(1,0)\leftarrow(1,0,0)}$ | $\sim 0$ |
| $P^A_{1\leftarrow Q}$ | $\sim 0$ | $W_{(0,1)\leftarrow(0,0,1)}$ |
| $P^A_{2\leftarrow Q}$ | $\sim 0$ | $\sim 0$ |

## Figure Captions

Figure 1. Adiabatic potential energy surfaces $\epsilon_n(\vec{R})$ and $\epsilon_{n+1}(\vec{R})$ from diagonalization of the electronic Hamiltonian, $\hat{H}_e$ ( ····· ). Diabatic potential energy surfaces $\tilde{\epsilon}_Q(\vec{R})$ and $\tilde{\epsilon}_D(\vec{R})$, which cross, from a nondiagonal representation of $\hat{H}_e$ ( —— ).

Figure 2. Correlation diagram of several low-lying electronic states of $C_2N_2$ showing CN state products from collinear dissociation.

Figure 3. Character of dissociative pathway. $C_2N_2(\tilde{C}\ ^1\Pi_u)$ is an $n \rightarrow \pi^*$ transition from the ground state, whereas $CN(X\ ^2\Sigma^+) + CN(A\ ^2\Pi)$ is a $\pi \rightarrow \sigma^*$ transition. Initial approach of $CN(X\ ^2\Sigma^+)$ and $CN(A\ ^2\Pi)$ fragments is a repulsive interaction.

Figure 4. Bond lengths and frequencies versus $\rho$ for $CN(X\ ^2\Sigma^+)$ and $CN(A\ ^2\Pi)$ states from *ab initio* MCHF minimal basis set calculations for the minimum energy path for collinear dissociation of $C_2N_2(\tilde{C}\ ^1\Pi_u)$.

Figure 5. Section of calculated diabatic electronic potential energy surfaces. The solid line indicates energy of 164 nm photon. Crossing point occurs at 8.9 eV which is 1.4 ev above 164 nm photon energy.

Figure 6. $CN(X\ ^2\Sigma^+)$ Vibrational Distributions. Calculated O and experimental ◇ relative PVDs for $CN(X\ ^2\Sigma^+)$ at wavelengths studied by Jackson et al. Computed results obtained for $A = 2.4 \cdot 10^9\ cm^{-1}$ at all energies, and $\gamma = 4.88\ Å^{-1}$ at 164 nm, $\gamma = 4.81\ Å^{-1}$ at 158.7 nm, and $\gamma = 4.64\ Å^{-1}$ at 153.6 nm; see Eq. (33).

Figure 7. Effective Potentials for Transitions at 164 nm. Calculated electronic potential for minimum energy path (—— ). Labeled curves indicate effective potentials for transitions to fragment states $(\nu_X, \nu_A)$ for $A = 2.4\ 10^9\ cm^{-1}$ and $\gamma = 4.88\ Å^{-1}$; see Eq. (33).

Figure 8. Computed $CN(X\ ^2\Sigma^+)$ and $CN(A\ ^2\Pi)$ PVDs at 164 nm. O - initial quasidiscrete state with one quantum in the symmetric CN stretch. ◇ -initial state with one quantum in the asymmetric CN stretch.

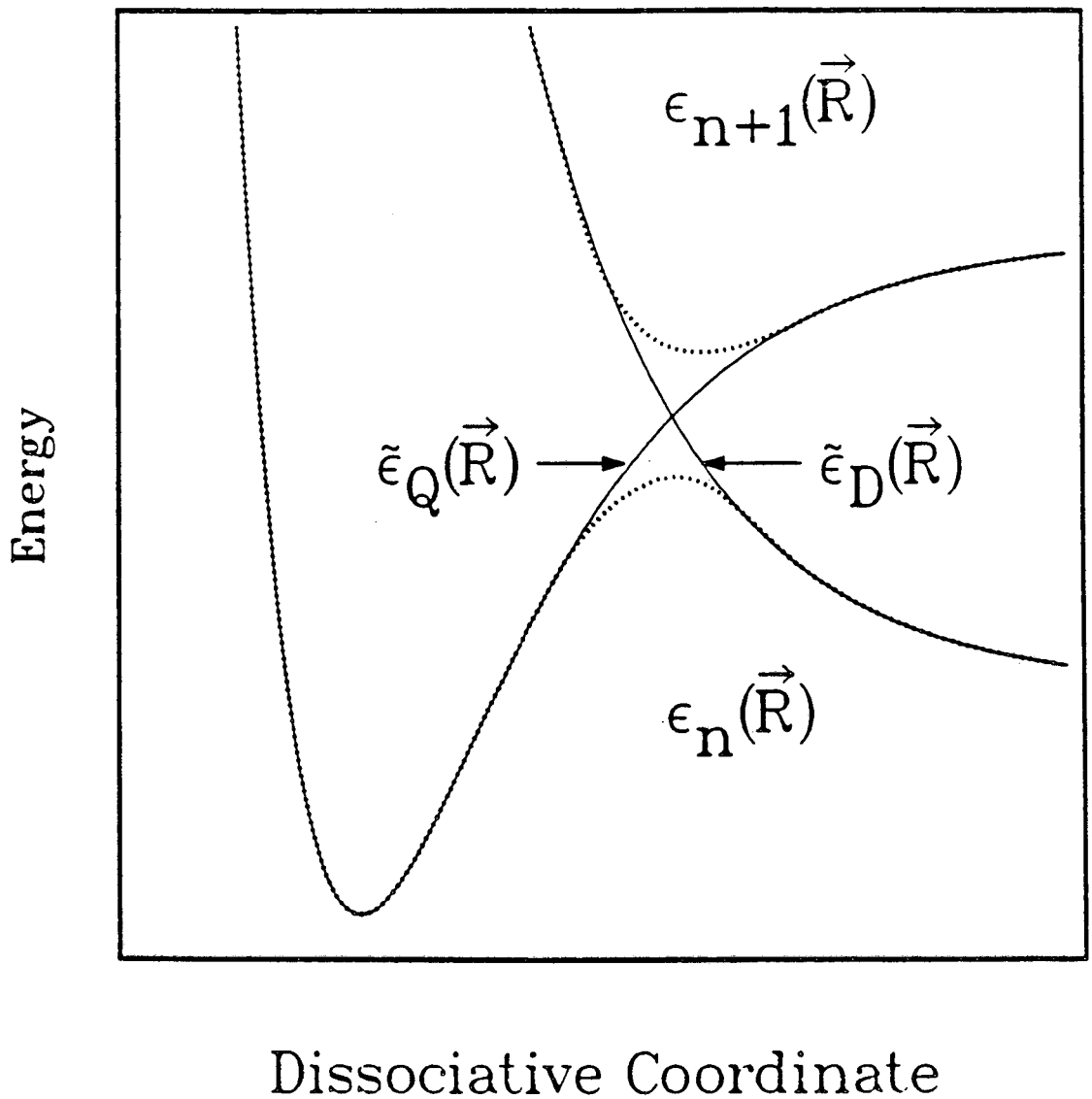


XBL 867-2810

FIGURE 1.

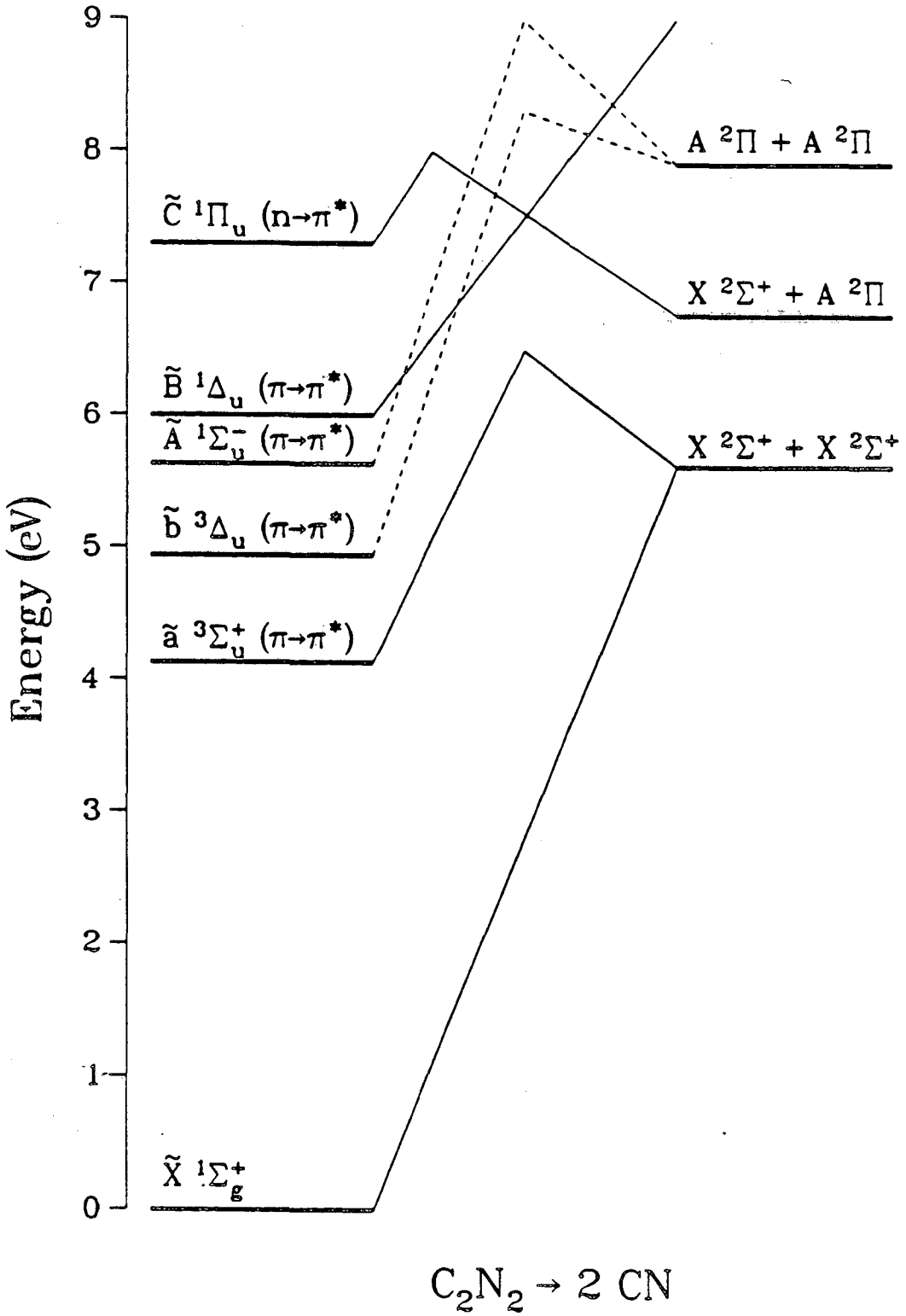


XBL 867-2811

FIGURE 2.

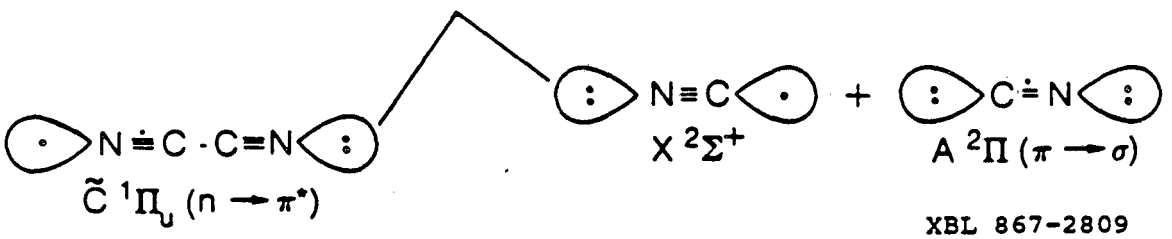


XBL 867-2809

FIGURE 3.

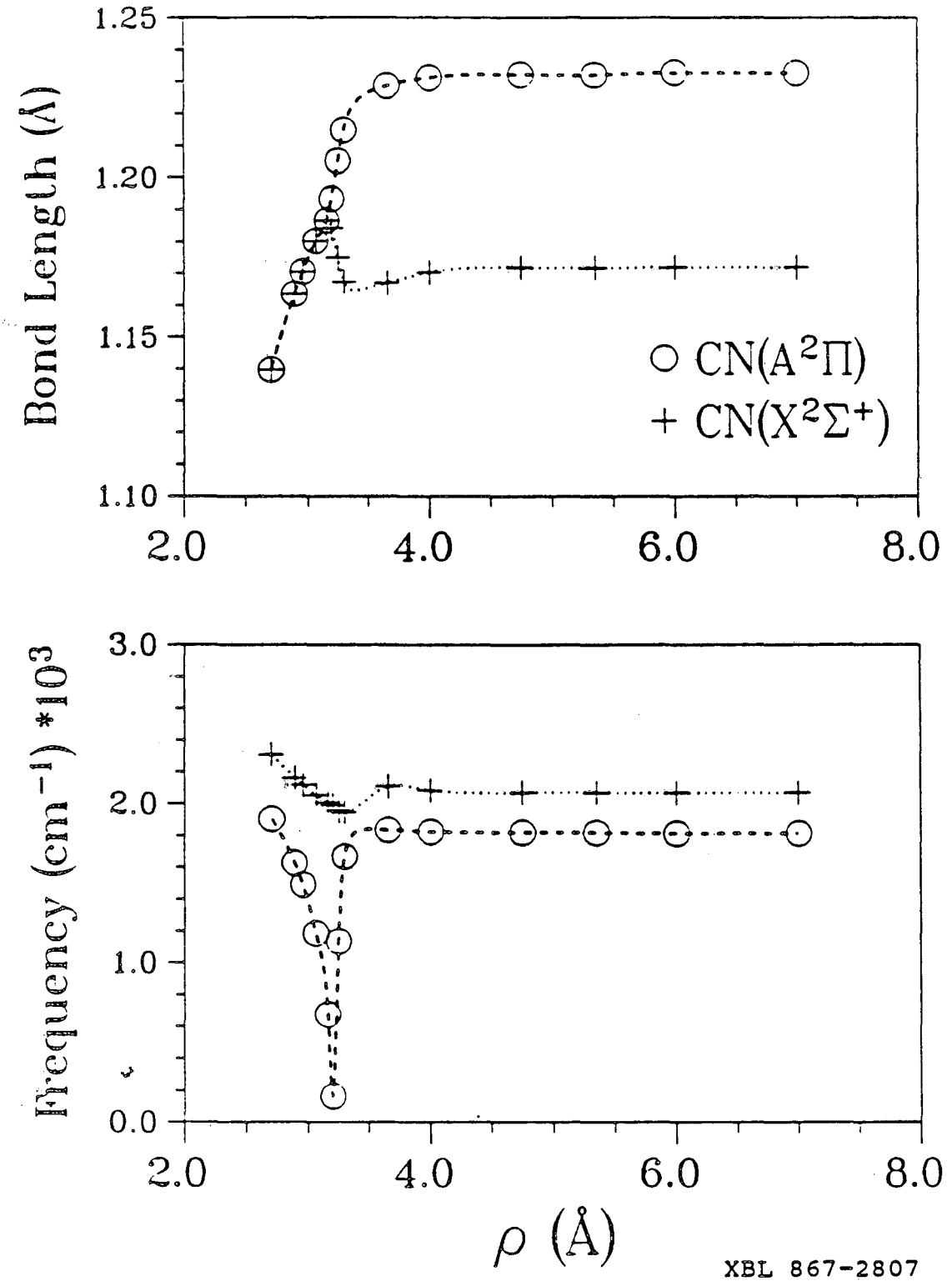
1.25
1.20
1.15
1.10
Bond Length (Å)
○ CN(A²Π)
+ CN(X²Σ⁺)
2.0
4.0
6.0
8.0
3.0
2.0
1.0
0.0
Frequency (cm⁻¹) *10³
ρ (Å)
XBL 867-2807

FIGURE 4.

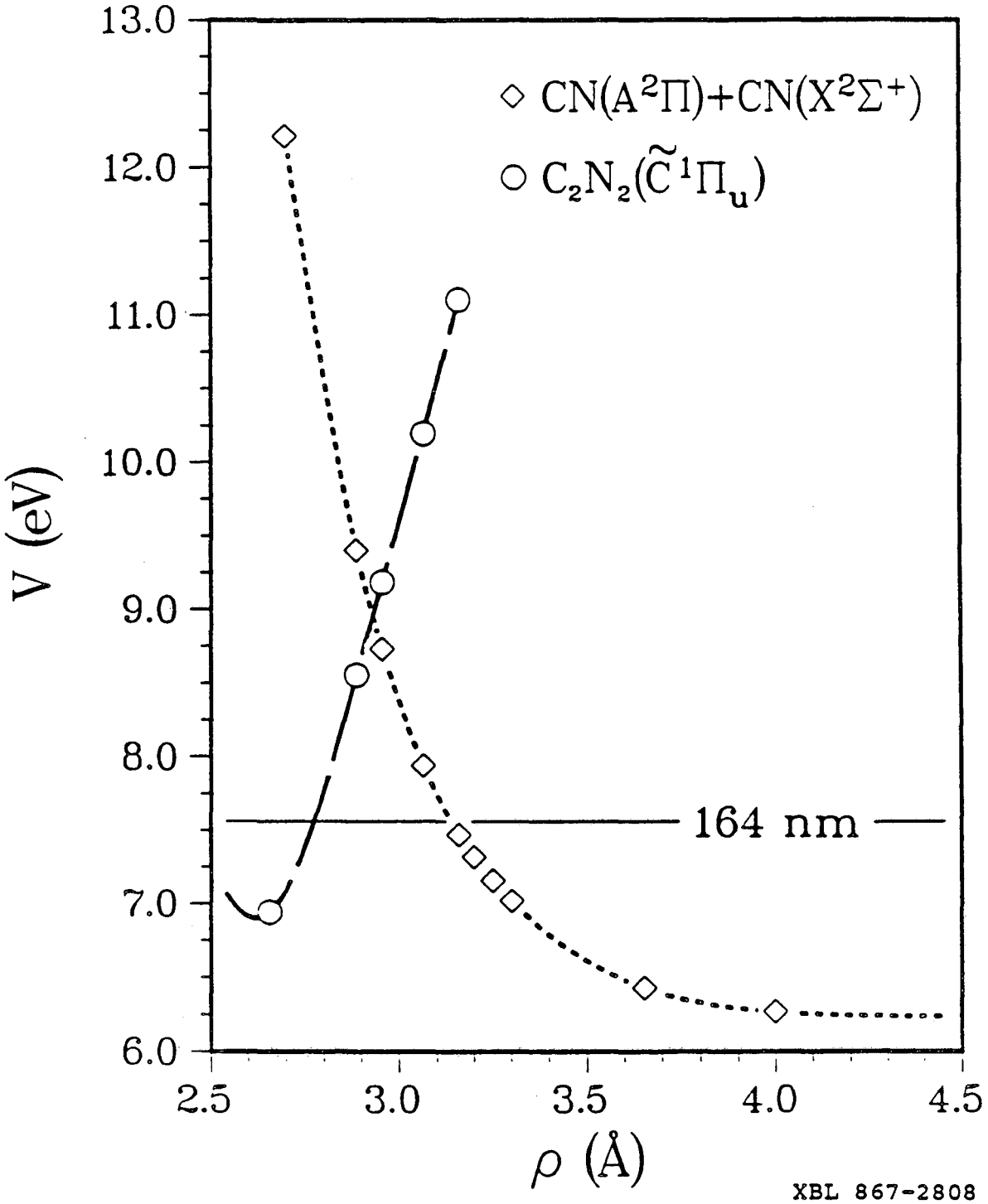
13.0
12.0
11.0
10.0
9.0
8.0
7.0
6.0
V (eV)
◇ CN(A²Π)+CN(X²Σ⁺)
○ C₂N₂(C̃¹Πu)
164 nm
2.5
3.0
3.5
4.0
4.5
ρ (Å)
XBL 867-2808

FIGURE 5.

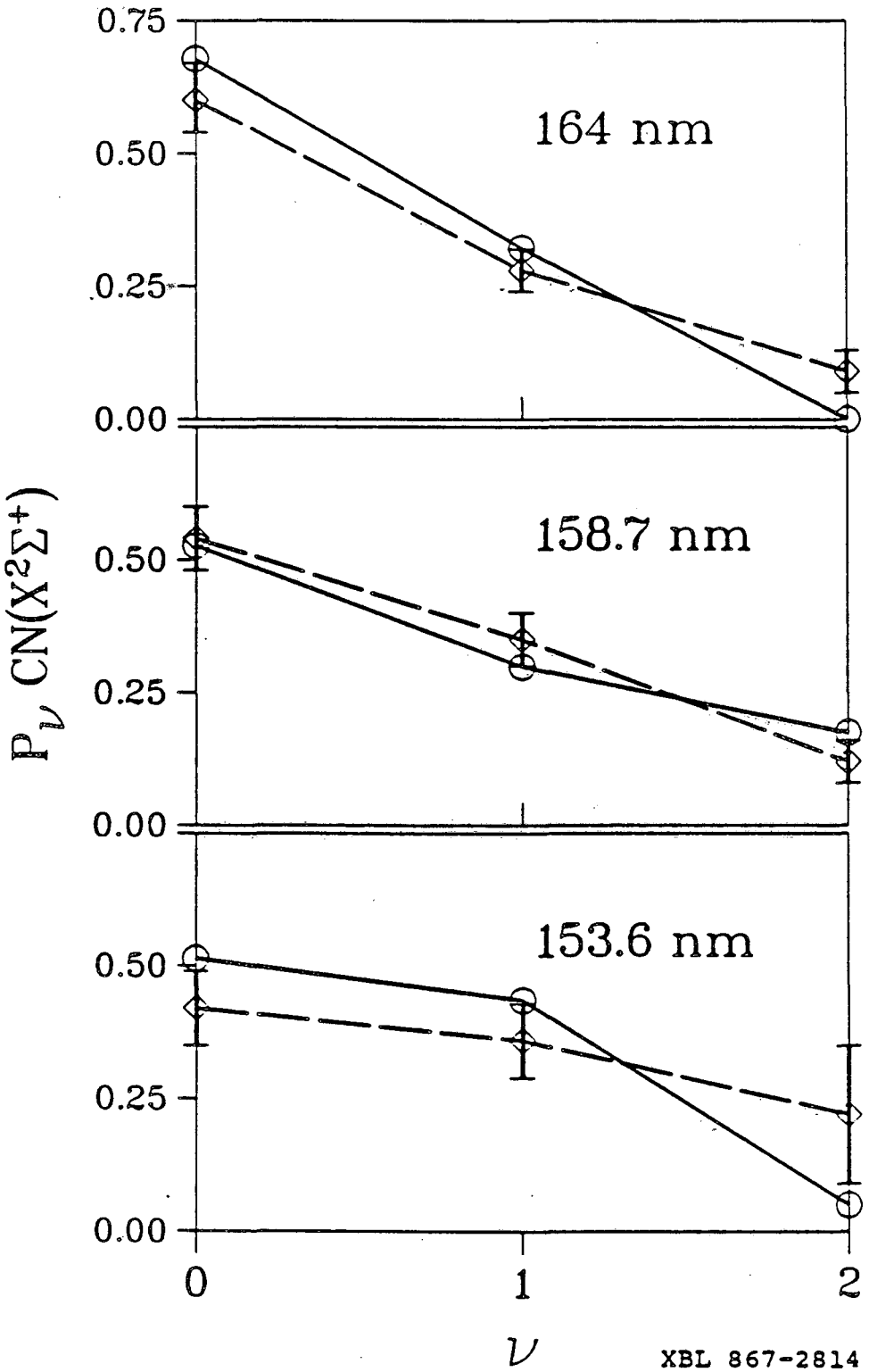
0.75
0.50
0.25
0.00
164 nm
158.7 nm
153.6 nm
$P_\nu$ CN($X^2\Sigma^+$)
0
1
2
$\nu$
XBL 867-2814

FIGURE 6.

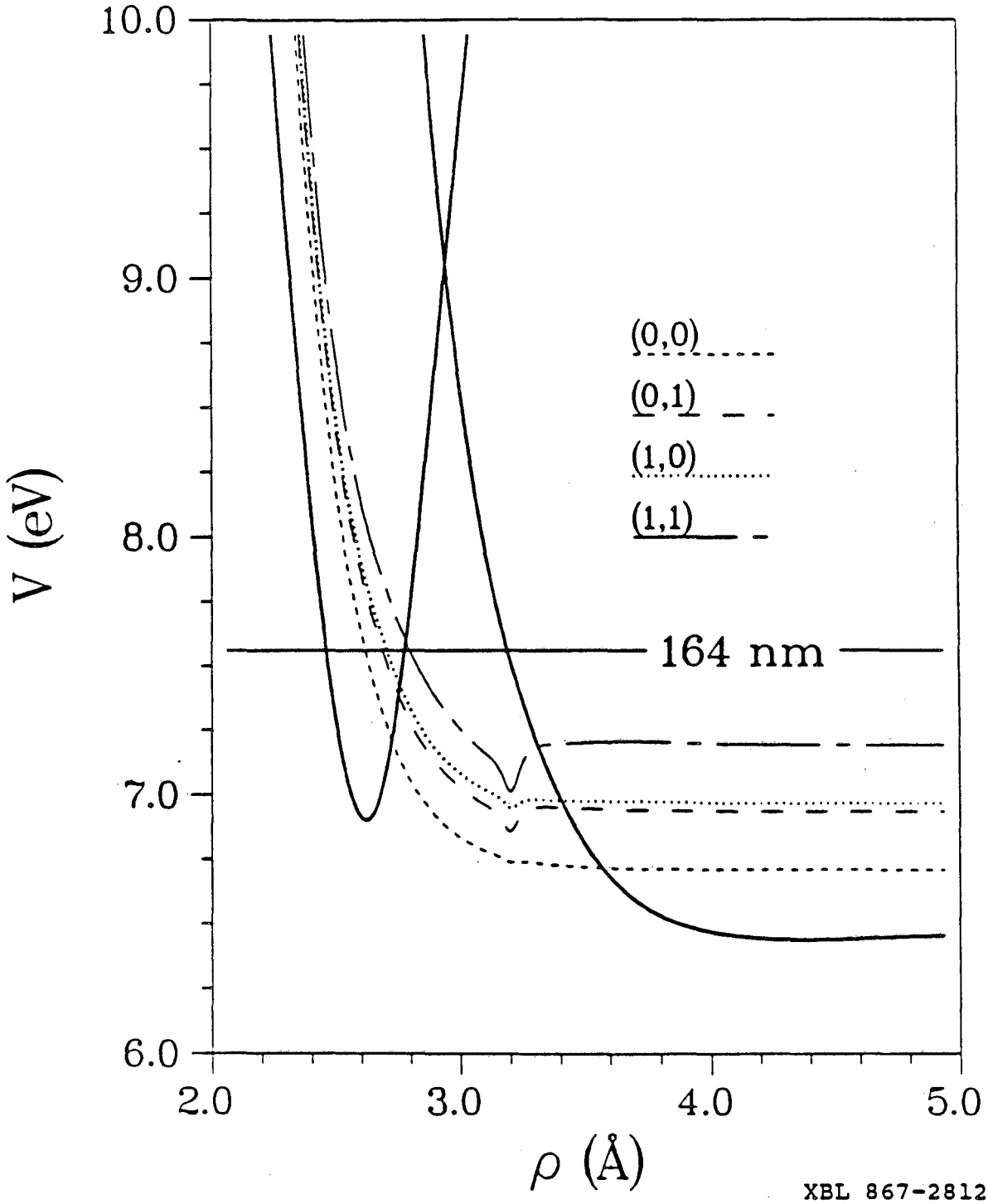


FIGURE 7.

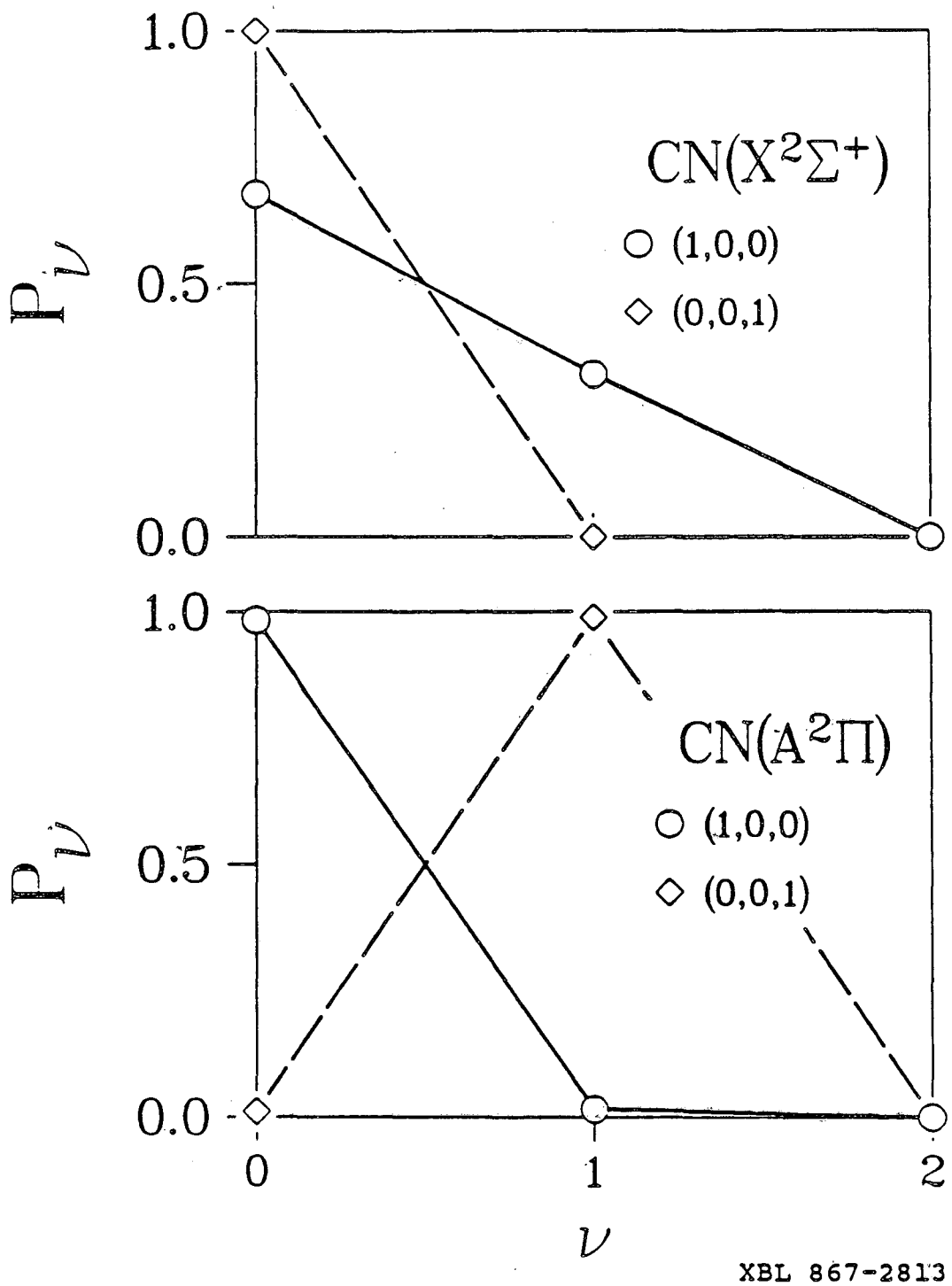


XBL 867-2813

FIGURE 8.

This report was done with support from the Department of Energy. Any conclusions or opinions expressed in this report represent solely those of the author(s) and not necessarily those of The Regents of the University of California, the Lawrence Berkeley Laboratory or the Department of Energy.

Reference to a company or product name does not imply approval or recommendation of the product by the University of California or the U.S. Department of Energy to the exclusion of others that may be suitable.

*LAWRENCE BERKELEY LABORATORY*
*TECHNICAL INFORMATION DEPARTMENT*
*UNIVERSITY OF CALIFORNIA*
*BERKELEY, CALIFORNIA 94720*